



## Timing and tempo of organic carbon burial in the Monterey Formation of the Santa Barbara Basin and relationships with Miocene climate

Eliel S.C. Anttila <sup>a,\*</sup>, Francis A. Macdonald <sup>a</sup>, Dawid Szymanowski <sup>b,c</sup>, Blair Schoene <sup>b</sup>, Andrew Kylander-Clark <sup>a</sup>, Clara Danhof <sup>d</sup>, David S. Jones <sup>d</sup>

<sup>a</sup> Department of Earth Science, University of California Santa Barbara, 1006 Webb Hall, Santa Barbara, CA, 93117, United States of America

<sup>b</sup> Department of Geosciences, Princeton University, Guyot Hall, Princeton, NJ, 08544, United States of America

<sup>c</sup> Institute of Geochemistry and Petrology, ETH Zurich, Clausiusstrasse 25, 8092 Zurich, Switzerland

<sup>d</sup> Department of Geology, Amherst College, Beneski Building, Amherst, MA, 01002, United States of America



### ARTICLE INFO

#### Article history:

Received 19 May 2023

Received in revised form 31 July 2023

Accepted 2 August 2023

Available online xxxx

Editor: A. Jacobson

Dataset link: [https://github.com/eliel-anttila/Anttila\\_Monterey\\_2023](https://github.com/eliel-anttila/Anttila_Monterey_2023)

#### Keywords:

Monterey Formation  
Miocene climate  
organic carbon burial  
U-Pb geochronology

### ABSTRACT

Understanding the transfer of carbon between Earth's surface reservoirs is necessary for interpreting climate transitions in Earth history and predicting future climate change. Warming associated with the 16.9–14.7 Ma Miocene Climate Optimum and subsequent cooling during the 14.7–13.8 Ma Middle Miocene Climate Transition provide opportunities to study carbon cycle dynamics in the geologically recent past. The Monterey Hypothesis interprets the Middle Miocene Climate Transition cooling as part of a positive feedback in which enhanced organic carbon burial on the eastern Pacific margin drew down atmospheric CO<sub>2</sub>. This idea has been supported by the correlation of organic-rich deposits in the Monterey Formation in coastal California with the mid-Miocene Monterey Event, a globally-observed positive shift in the δ<sup>13</sup>C of marine carbonates that may be indicative of elevated burial of δ<sup>13</sup>C-depleted organic carbon. Here, we use 31 new U-Pb zircon laser ablation inductively coupled plasma mass spectrometry ages and 14 new isotope dilution thermal ionization mass spectrometry ages from volcanic ash beds in the Monterey Formation along the Santa Barbara coast to constrain the timing and tempo of organic carbon mass accumulation in some of the most organic-rich rocks in California. The new age model demonstrates that peaks in organic carbon mass accumulation rate in the Monterey Formation do not coincide with the Monterey Event, and that total organic carbon content in the Miocene Santa Barbara Basin is inversely correlated with sedimentation rate. We propose that changes in organic carbon burial rates in the Monterey Formation were driven by a combination of sea-level change and local tectonically-mediated basin formation, which provided first-order controls on sedimentation rate, and that organic carbon burial in the Monterey Formation is better described as a response to, rather than a driver of, global climate.

© 2023 The Author(s). Published by Elsevier B.V. This is an open access article under the CC BY license (<http://creativecommons.org/licenses/by/4.0/>).

### 1. Introduction

Organic-rich strata of the Monterey Formation were deposited in borderland basins along the western margin of North America during the Miocene, and are the primary source and reservoir rocks for California's hydrocarbon resources (Bramlette, 1946; Pisaciotto and Garrison, 1981; Behl et al., 1999). Although the burial and preservation of organic material in the Monterey Formation has been investigated for more than half a century, attribution of the specific global and local processes that resulted in the distri-

bution of organic-rich rocks in California remains a subject of debate. Deposition of the Monterey Formation spanned the Miocene Climatic Optimum [MCO, marked by peak Neogene temperatures (Modestou et al., 2020) and a nadir of Antarctic ice extent (Foster et al., 2012)] through onset of the subsequent global cooling trend (Westerhold et al., 2020; Holbourn et al., 2014), motivating the hypothesis that organic carbon burial in the Monterey Formation and temporally-equivalent units in the eastern Pacific drove Miocene climate change (Vincent and Berger, 1985; Flower and Kennett, 1993). Conversely, other workers have suggested that the MCO was marked by low marine organic carbon burial rates (Li et al., 2023; John et al., 2002), consistent with hypotheses suggesting that local preservation factors, rather than enhanced organic production and burial, were responsible for the elevated organic content of Mon-

\* Corresponding author.

E-mail address: [eanttila@ucsb.edu](mailto:eanttila@ucsb.edu) (E.S.C. Anttila).

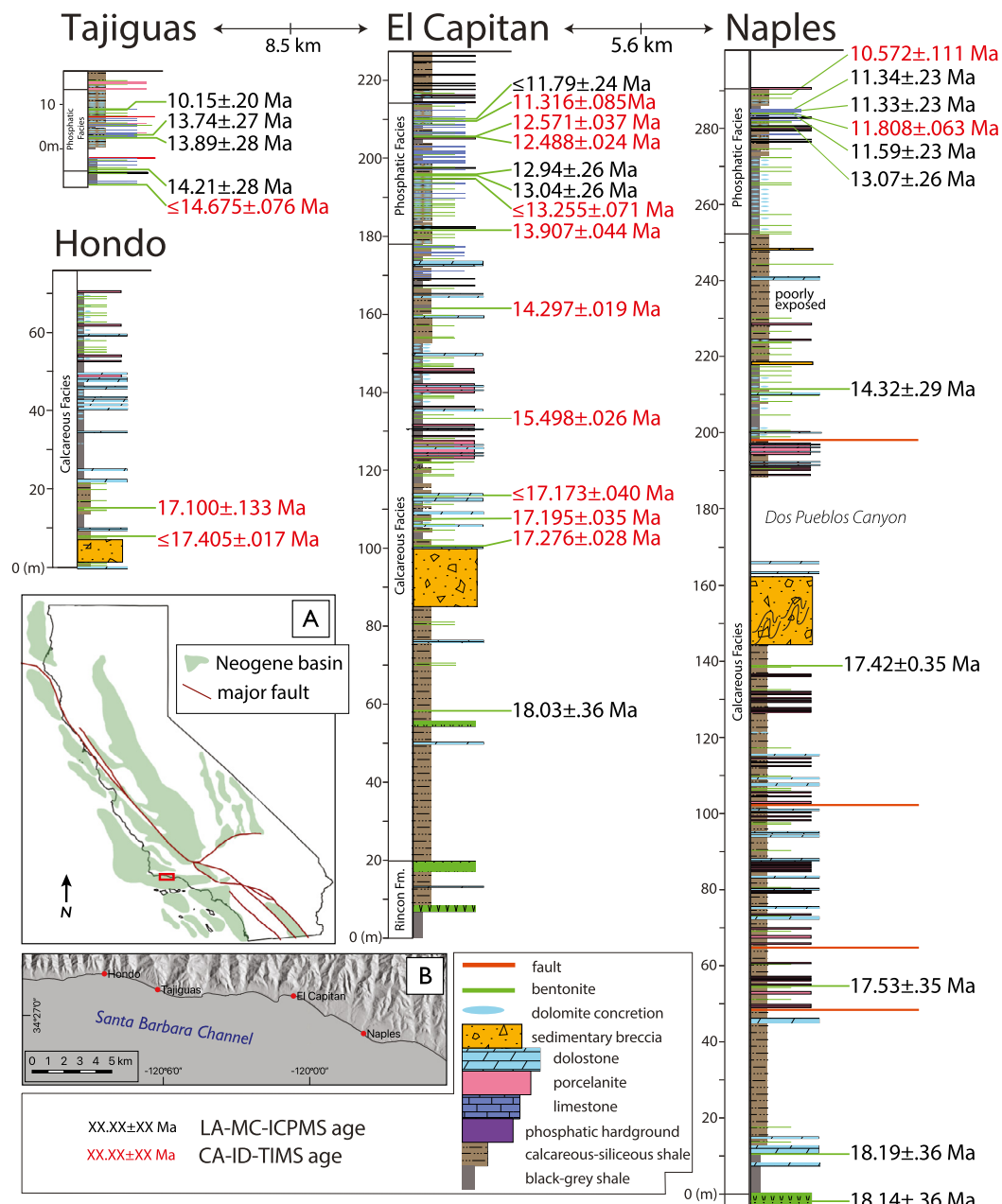


**Fig. 1.** A) Neogene sedimentary basins of California, modified from Behl (1999), with study area highlighted in red and expanded in B). C) Stratigraphic sections through outcrops at four beach-cliff exposures of the Monterey Formation, with U-Pb zircon ages appended onto the bentonites from which they were derived. Maximum depositional ages are represented with a  $\leq$ .

terey Formation shales (Isaacs, 1984; John et al., 2002; Föllmi et al., 2005).

These hypotheses can be assessed by quantifying the rate and timing of organic carbon burial in the Monterey Formation. Existing age models for the Monterey Formation rely primarily on biostratigraphy (John et al., 2002; Föllmi et al., 2005), with secondary constraints from chemostratigraphy and magnetostratigraphy. However, evidence of reworking and sedimentary condensation (Föllmi et al., 2005) complicates age assignment, as does variable preservation of calcareous skeletal material (Barron, 1986) and limited absolute age calibration for Californian marginal biozones (Crouch and Bukry, 1979). Carbon and oxygen isotope chemostratigraphic correlations of the Monterey Formation to global records (Flower and Kennett, 1993) are compromised by carbonate authigenesis (Blättler et al., 2015), and basin restriction (Isaacs et al., 2001; Hancock et al., 2019).

Here, we present precise U-Pb geochronology on zircon derived from volcanic ash beds intercalated within Monterey Formation strata. These dates anchor age models through four stratigraphic sections along the northern edge of the Santa Barbara Channel (Fig. 1). At the El Capitan and Naples sections, age models are paired with both new and previously published total organic carbon (TOC) measurements to constrain the rate of organic carbon burial. All age models are then integrated into a basinal chronostratigraphy to assess the synchronicity of lithostratigraphic change across the Santa Barbara Basin (SBB) and to consider mechanisms for driving the accumulation of organic carbon. Within this chronostratigraphic framework, changes in TOC abundance and organic carbon mass accumulation rate (OCMAR) are compared with putative far-field drivers, and are used to assess the relationships between organic carbon burial in the Monterey Formation and Miocene climate change.

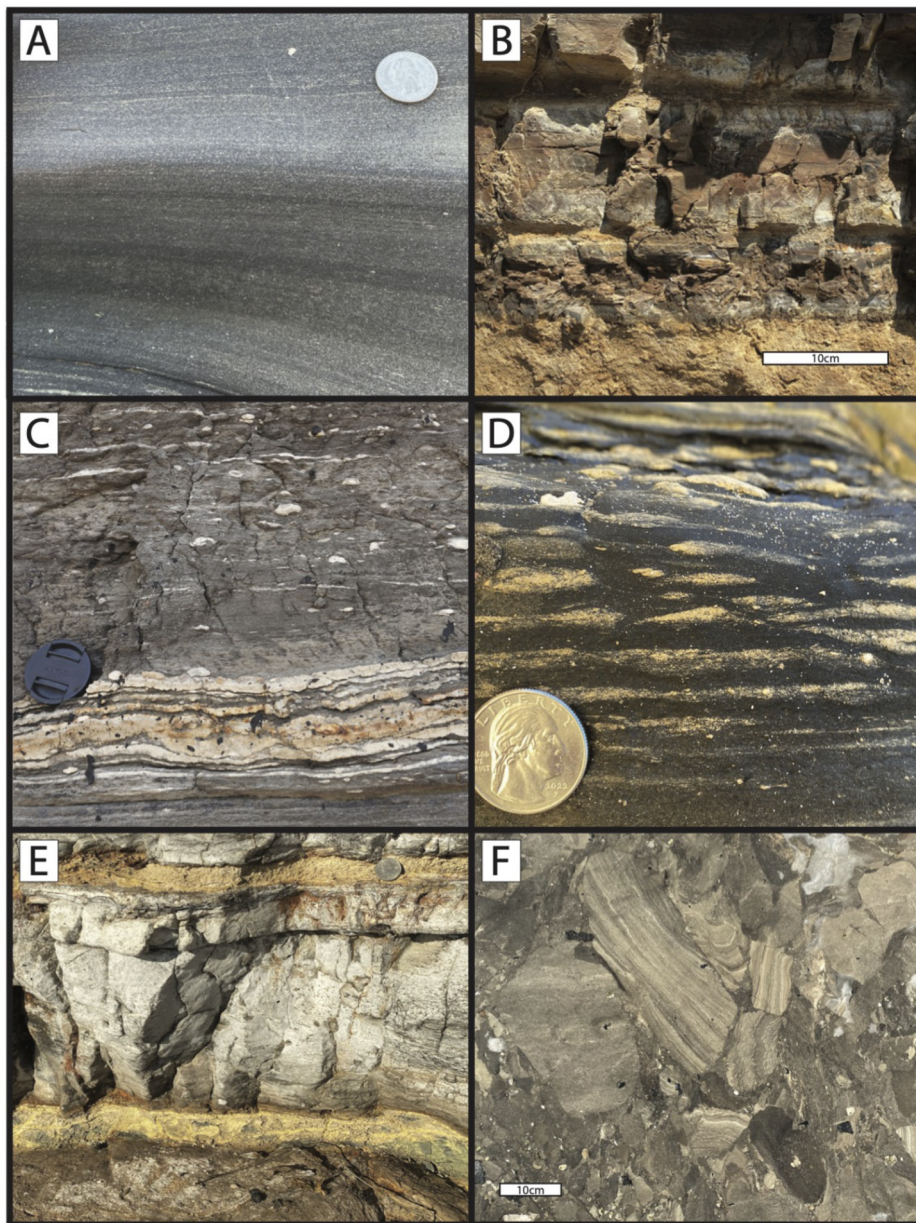


**Fig. 2.** Field photographs of Monterey Formation outcrops from the Santa Barbara Basin. A) laminated shales, Tajigus. Smaller, homogeneously distributed light specks are foraminifera and other calcareous fossil material, while larger white grains are angular granule-sized clasts of remobilized authigenic phosphate or dolomite. B) Massive shale (bottom) overlain by laminated porcelanite, middle Naples. C) Condensed phosphatic interval, Tajigus Beach. Continuous white layers are lag deposits of authigenic phosphatic clasts cemented by additional phosphatic material. Note dispersed authigenic phosphate nodules in relatively expanded shale above the condensed horizons. D) reworked angular phosphatic grains in cross bedded shale matrix, Naples. High concentrations of phosphatic grains typically host secondary phosphatic cements. E) Bentonites in outcrop at Tajigus, weathering yellow-to-ochre and separated by dark calcareous shale with a characteristic light gray weathering rind. Upper ash is EAGC2014, which sits at 3.0 m in the composite Tajigus section (Fig. 1). F) Detail of the block breccia horizon, Naples. Note variable folding of reworked shale clasts, indicating variable lithification of the source shales prior to remobilization.

## 2. Geological background

The Monterey Formation of the SBB outcrops in beach cliff exposures along the northern edge of the Santa Barbara Channel (Fig. 1B; Isaacs, 1981). Shale, carbonate, and porcelanite (porous opaline silica) of the Monterey Formation broadly expand eastward with lateral variability in both thickness and facies over sub-km to km-scales, consistent with deposition within an active, fault-bounded transtensional borderland basin (Luyendyk et al., 1980). The thickness and facies changes within these coastal outcrops are a manifestation of similar variability spanning the greater SBB: the outcrops on the northern channel coast represent the condensed, banktop-proximal equivalents of thicker, siliceous basinal facies of

the central Santa Barbara Channel (Hornafius, 1991). These basinal deposits are bounded to the south by another paleotopographic high (Isaacs, 1984), which now forms the Santa Barbara Channel Islands.

The Monterey Formation is subdivided into three lithostratigraphic units: the Calcareous Facies, Phosphatic Facies, and Siliceous Facies (Pisciotto and Garrison, 1981). The basal Calcareous Facies rests above the Rincon Shale and consists of calcareous-siliceous shales (Fig. 2A), interspersed with minor dolostone and porcelanite (Fig. 2B). The overlying Phosphatic Facies features darker, organic carbon-rich shale with abundant authigenic phosphatic and dolomitic nodules (Fig. 2C), reworked deposits of authigenic material (Fig. 2D), concentrated phosphorite beds (Fig. 2C), and rare

lenticular dolomite (John et al., 2002; Föllmi et al., 2005; Isaacs et al., 2001; Bohacs and Schwalbach, 1994). The uppermost Siliceous Facies is dominated by largely-featureless porcelanite beds, interrupted by subsidiary shale and marl horizons (Isaacs et al., 2001; Laurent et al., 2015).

The relative abundance of the biogenous, terrigenous, and authigenic components of the Monterey Formation can vary on centimeter scales within individual vertical sections (John et al., 2002; Föllmi et al., 2005) and on decimeter to kilometer scales along strike, following the compositional and facies variability described above. Bulk sedimentation rates broadly represent a combination of terrigenous and biogenous sediment fluxes to the depozone, with changes in the relative magnitude of these fluxes (as well as post-depositional authigenesis) resulting in the lithological variability observed throughout all three facies. Although the Miocene SBB was relatively distal from the continental margin, outer borderland paleotopographic highs (Hornafius, 1991; Marsaglia et al., 2006) may have provided local sediment sources, potentially augmented by fine current-borne suspended terrigenous material from the continental margin (as observed in the modern Tanner Basin; Gorsline et al., 1968). Most shales within the Miocene SBB contain between ~20–50% terrigenous detrital material (Föllmi et al., 2005; Laurent et al., 2015). However, abundant Type II kerogen suggests a primarily marine origin for organic carbon in the Monterey Formation (Laurent et al., 2015). The occurrence of dominantly biogenous rocks, such as porcelanites and cherts, has been previously attributed to either exceptional productivity (Barron, 1986; Pisciotti and Garrison, 1981), or to punctuated episodes of high biogenous flux during periods of relatively minimal terrigenous input, resulting in less dilution of the biogenous material (Isaacs, 1984). Reworking and remobilization of these components must also be considered, as the removal of fine-grained material by winnowing currents and slumping/mass wasting events played a major role in concentrating coarser authigenic material, as evidenced by reworked, clast-supported beds of nodular phosphate within the Phosphatic Facies (Fig. 2C; John et al., 2002; Föllmi et al., 2005; Laurent et al., 2015).

In the SBB, all three facies are intercalated with volcanic ash beds, most of which have been altered to bentonite clay (Fig. 2E), that range from <1 cm to >1 m thick. Bentonites outcrop as recessive ochre, maroon, green, or blue-gray lamina within the surrounding strata. Some ashes in the SBB have been mineralogically or geochemically correlated within the SBB (Hornafius, 1994) and with potential eruptive sources (Knott et al., 2022), but few ash beds from the SBB have been dated with U-Pb geochronology (Fenton, 2018).

### 3. Methods

Between 2018 and 2021, stratigraphic sections were measured at multiple Monterey Formation outcrop localities on the northern edge of the Santa Barbara Channel. Within each section, bentonites were collected for U-Pb geochronology, with ~0.5 kg of sample collected from each horizon. All geochronological sample locations are compiled in Table SM1. At the El Capitan section, shales were collected for TOC and XRF analysis at ~1 m intervals in the lower 100 m of the section, and at ~30 cm intervals in the upper portion of the section. Sampling targeted fresh surfaces with minimal weathering rind (which are abundant due to active cliff retreat), and without visual evidence of hydrocarbon migration. Zircons from geochronological samples were dated with laser ablation-inductively coupled plasma mass spectrometry (LA-ICPMS), and a subset of zircons from fourteen samples were dated with chemical abrasion-isotope dilution-thermal ionization mass spectrometry (CA-ID-TIMS). El Capitan shale samples were powdered and compositionally analyzed with a handheld XRF, and an aliquot of each

sample was decarbonated and analyzed for TOC content. Full descriptions of geochronological and geochemical analyses are available in the attached Supplementary Material.

## 4. Results

### 4.1. Geochronology and age model

LA-ICPMS U-Pb dating resolved statistically-significant young magmatic zircon populations from 31 bentonite samples from the Monterey Formation. All weighted-mean ages calculated from these populations are stratigraphically consistent (younging upward), within  $2\sigma$  uncertainty (Figs. 1, 3). 14 samples also analyzed with CA-ID-TIMS yielded modeled eruptive ages that are stratigraphically consistent and indistinguishable, within uncertainty, from LA-ICPMS weighted mean ages calculated for the same sample (Fig. 4A). The equivalence of LA-ICPMS and CA-ID-TIMS ages across all dually-measured samples suggests that despite differences in precision (Fig. 3), ages developed using both analytical techniques may be directly compared. Ages utilized in the chronostatigraphic framework are summarized in Fig. 1.

Discrete bentonite beds without visible bedding structures were sampled for geochronology. Although these horizons are interpreted to have formed primarily as the result of volcanic airfall, some horizons were likely reworked during and soon after deposition, as corroborated by older detrital tails on all LA-ICPMS age spectra. Older grains are expected in airfall tuffs falling into an active siliciclastic depozone, either as inherited grains incorporated before or during eruption, or as detrital grains. For the LA-ICPMS data, the youngest coherent population of zircons derived from each bentonite is interpreted as the eruptive age of the ash horizon. However, CA-ID-TIMS analyses revealed variability within the uncertainty envelope of weighted mean-LA-ICPMS ages, including samples where the youngest dated grain is statistically distinct from the rest of the population. For these samples, the age of the youngest grain precisely analyzed with CA-ID-TIMS is treated as a maximum depositional age (MDA, Fig. 1).

Ages from El Capitan and Naples were input into a stratigraphic Markov-Chain Monte Carlo (MCMC) model in the Chron.jl package (Schoene et al., 2019). Four ash ages from El Capitan were correlated with specific ash horizons at Naples Beach based on previously described tephrochronological (Hornafius, 1994), biostratigraphic (John et al., 2002; Föllmi et al., 2005), and lithostratigraphic similarities between sections. These ages were incorporated into the Naples age model with additional ( $\pm 1.5$  m) vertical uncertainty to account for potential miscorrelation. For horizons with multiple age constraints (e.g. a TIMS modeled eruptive age and a LA-ICPMS weighted mean age), the age with the least analytical uncertainty was chosen as the model constraint. For the three horizons at El Capitan where a weighted-mean or modeled-eruptive age was not calculated (due to a distinct young grain in a LA-ICPMS sample, or a single young grain in a group of TIMS analyses), the resultant MDA was utilized in the age model. All ages utilized in the Chron.jl framework are in bold text in Table SM1, and depicted in Fig. 1. The model was run at a vertical resolution of 0.2 m, with 30,000 steps (10,000 runs discarded for burn-in), and 95% credible intervals were calculated (Figs. 4B, 5A).

Sedimentation rates and 68% credible intervals (Fig. 4D, 5C) were calculated in the Chron.jl age-height model framework using an overlapping binned approach. Here, we utilize a shifting bin size of  $(age)/10$ , with a 10-bin overlap in order to minimize spurious spikes or rapid transitions in sedimentation rate observed with narrower bins. Regardless of the binning method, the trends and mean modeled sedimentation rates are comparable, and consistently approach values expected for linear sedimentation rates between age constraints.

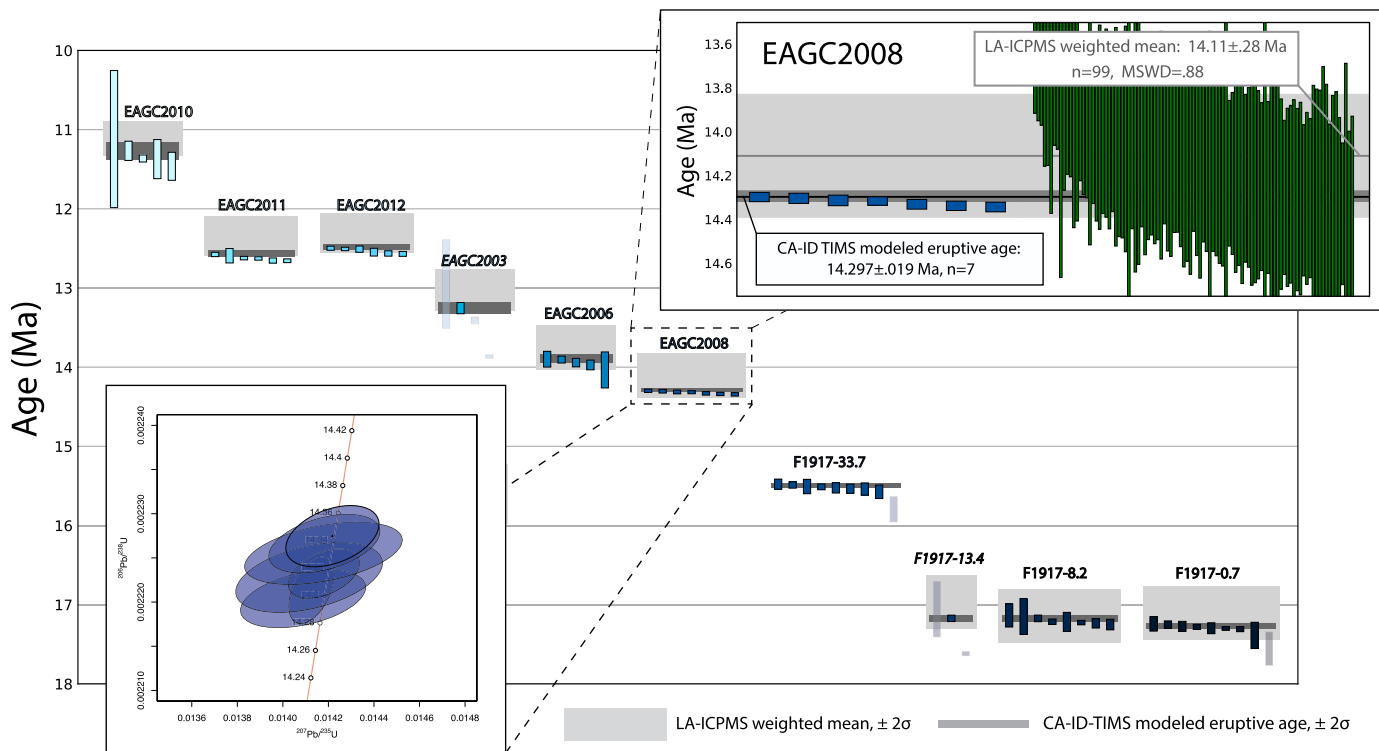


**Fig. 3.** Th-corrected  $^{206}\text{Pb}$ - $^{238}\text{U}$  dates, with  $2\sigma$  uncertainty, from all zircons analyzed by CA-ID-TIMS from El Capitan, grouped by sample and plotted vs. age. Modeled TIMS eruptive ages (dark gray bars) and LA-ICPMS weighted-mean ages from each sample (light gray bars) are shown behind each group of individual analyses. Italicized labels indicate a sample for which TIMS analyses yielded a single young grain with good analytical precision, resulting in the characterization of the resultant TIMS age for that sample as a maximum depositional age for the sampled bentonite horizon. Left inset shows a Wetherill concordia plot of all CA-ID-TIMS analyses from sample EAGC2008, while the inset panel at right details the age and uncertainty of all individual analyses (CA-ID TIMS in blue, LA-ICPMS in green) used to calculate the age of sample EAGC2008. A summary of all geochronological data, including concordia diagrams and weighted-mean plots for all measured samples, can be found in the Supplementary Materials.

#### 4.2. Organic carbon mass accumulation rate

TOC measurements on shales from El Capitan Beach range from 1–24 wt% TOC (Fig. 4C). The trends of this new dataset largely agree with earlier measurements from El Capitan by John et al. (2002), as well as with TOC datasets from Naples Beach (Fig. 5B; Föllmi et al., 2005; Isaacs et al., 2001, Bohacs and Schwalbach, 1994). TOC data from prior publications was integrated into our measured sections by matching tie points from the measured sections into our stratigraphic framework. For each measured section, an exponential moving average was calculated with the compiled TOC data in order to characterize trends in TOC abundance, and appended with a  $1\sigma$  analytical uncertainty envelope (Figs. 3C, 4B).

Organic carbon mass accumulation rate (OCMAR, mg/cm<sup>2</sup>/kyr) is calculated using the following equation:

$$\text{OCMAR} = S * C_{\text{tot}} * \rho \quad (1)$$

where  $S$  (m/Myr) is modeled sedimentation rate,  $C_{\text{tot}}$  (wt%) is organic carbon (in this case an exponential moving average of TOC measurements taken through the section), and  $\rho$  (g/cm<sup>3</sup>) is an assumed shale density of 2.1 g/cm<sup>3</sup>.  $1\sigma$  uncertainty is propagated using the following equation:

$$\frac{\sigma \text{OCMAR}}{\text{OCMAR}} = \sqrt{\left(\frac{\sigma S}{S}\right)^2 + \left(\frac{\sigma C_{\text{tot}}}{C_{\text{tot}}}\right)^2 + \left(\frac{\sigma \rho}{\rho}\right)^2} \quad (2)$$

where  $\sigma S$  is  $1\sigma$  uncertainty in sedimentation rate generated by Chron.jl;  $\sigma C_{\text{tot}}$  is 1.8%, the  $1\sigma$  analytical uncertainty associated with our TOC measurements, and  $\sigma \rho$  is 0.2 g/cm<sup>3</sup>, or the estimated  $1\sigma$  uncertainty associated with potential variability in shale density through the section. OCMARs for both El Capitan and

Naples are plotted both against stratigraphic height (Figs. 4E, 5D) and time (Fig. 6A).

Usage of post-compaction average shale density accounts for compaction-related change in both density and apparent sedimentation rate in OCMAR estimates. This is particularly important in porcelanite-dominated intervals (e.g. ~120–140 m at El Capitan and ~190–200 m at Naples): the thickness of porcelanites derived from diatomaceous biogenous material can be reduced by a factor of 7 from their depositional thickness (given an initial porosity of 90% at deposition and a post-burial porosity of 10%; Isaacs, 1984). However, a density of 2.5 g/cm<sup>3</sup>, the upper  $2\sigma$  bound of density estimates utilized in our OCMAR calculation, is roughly equivalent to a pure diatomaceous porcelanite at 6.5% porosity, which is significantly less than porosities for measured porcelanites in the SBB (Isaacs, 1983), and mitigates potential compaction-related underestimates of OC accumulation rate through this interval. Overall, our mean assumed density is higher than average shale density through the section, resulting in a conservative overestimate of MAR through each section, and bolstering the argument for relatively low rates of OC burial in the Miocene SBB. This overestimate is further enhanced in silica-dominated intervals by the preferential sampling of shale: silica-rich porcelanites were not targeted for TOC sampling, and as a result the calculated average TOC content through porcelanite-dominated intervals is likely an overestimate.

#### 4.3. Shale elemental abundances

The Al/Si ratio, Ti content, Ca content, and Si/Ti ratio of El Capitan shales are plotted against TOC content in Fig. 7. All XRF-derived elemental abundances of Al, Ca, Si, and Ti are compiled in Table S5. Al/Si ratios (Fig. 7B), a proxy for clay abundance and mineral surface area (Galy et al., 2007; Van Hoang et al., 2010),

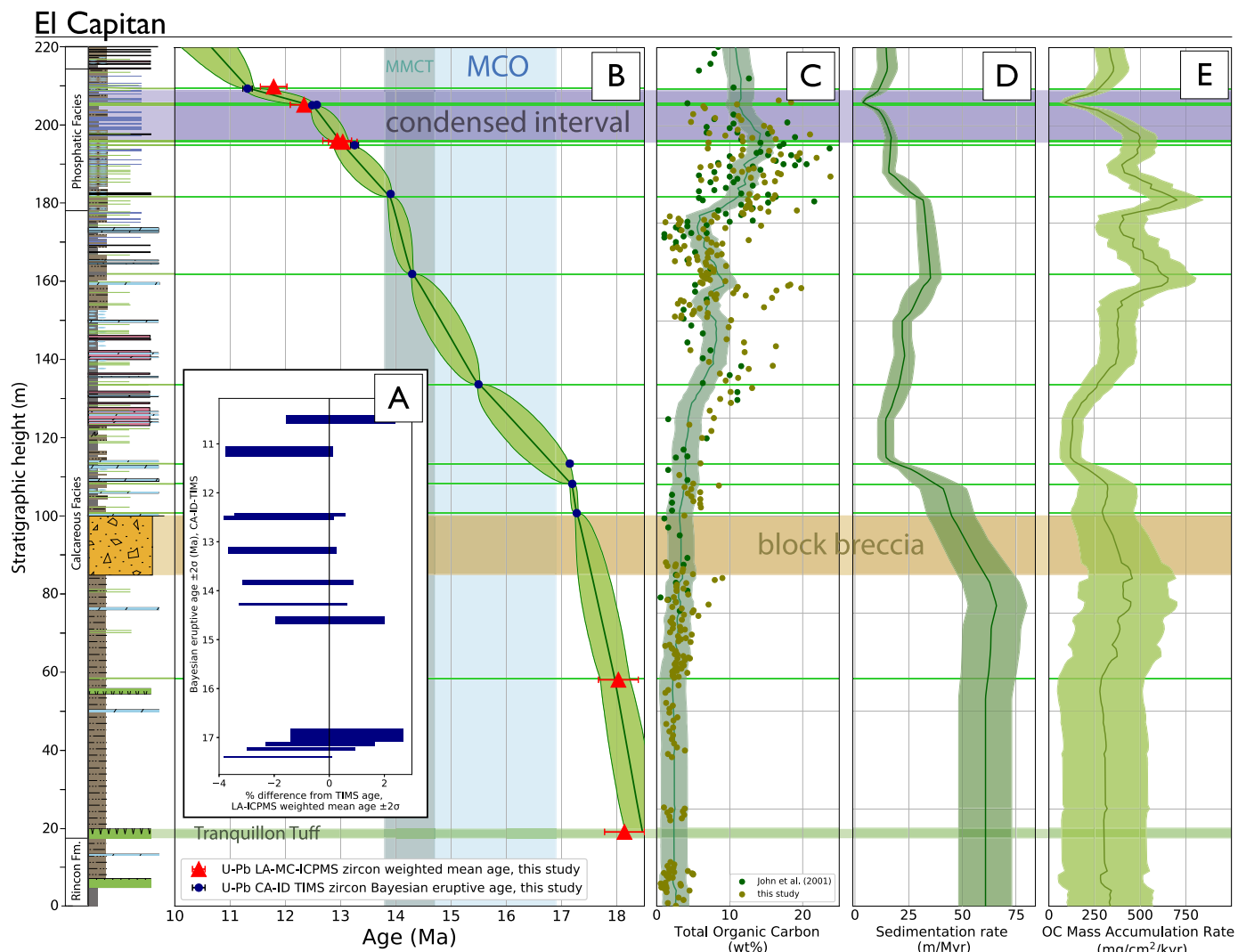


**Fig. 4.** Age model and modeled organic carbon mass accumulation rate (OCMAR) for El Capitan. A) CA-ID-TIMS ages vs. LA-ICPMS ages derived from the same bentonite sample, illustrating that both methods yield ages that may be directly compared. B) age vs. height model for El Capitan, showing the 95% credible interval envelope of modeled age-height relationships. Vertical bars illustrate the temporal extent of the Miocene Climatic Optimum (MCO) and mid-Miocene Climatic Transition (MMCT). C) Compiled total organic carbon (TOC) data (from this study and from John et al., 2002) from El Capitan, with a moving average through all data depicted as a solid line with  $1\sigma$  analytical uncertainty envelope. D) Modeled sedimentation rate for El Capitan, with 68% credible interval envelope. E) Modeled OCMAR curve and 68% credible interval envelope for El Capitan, plotted vs. stratigraphic height.

show a positive relationship with TOC content, as does Ti content (Fig. 7C), which is a redox-insensitive proxy for the abundance of terrigenous material in shale (Calvert and Pedersen, 2007). Meanwhile, both Ca abundance and the Si/Ti ratio have a broadly negative relationship with TOC (Fig. 7D, E). Ca serves as a proxy for  $\text{CaCO}_3$  abundance (Rothwell and Croudace, 2015), which, in Monterey Formation shales, is strongly influenced by the occurrence biogenous material (Föllmi et al., 2005). Si/Ti ratios indicate the relative prevalence of biogenous versus terrigenous silica sources, with higher ratios indicating a larger biogenous component (e.g. Agnihotri et al., 2008).

## 5. Discussion

### 5.1. Drivers of organic carbon accumulation in the Monterey Formation

High-TOC intervals within Monterey Formation sections of the SBB have been interpreted to represent enhanced organic carbon (OC) burial associated with upwelling-related increases in primary productivity (Flower and Kennett, 1993). This interpretation predicts synchronous increases in TOC and biogenous sediment flux

that are uncommon in the SBB, as evidenced by inverse relationships between biogenous proxies and TOC at El Capitan (Fig. 7C,D) and elsewhere (Föllmi et al., 2005; Laurent et al., 2015). Rather, TOC content is the result of the collective influence of several driving factors, including: 1) productivity, which delivers an initial flux of OC to the depozone; 2) dilution, which reduces the relative portion of organic carbon in a sediment through the deposition of non-organic material, and 3) preservation, which results in the survival and retention of only a fraction of initially-deposited OC. Although syn- and early-post-depositional preservational processes may have been important in modulating TOC content at El Capitan and Naples, evidence of minimal burial diagenesis at both localities (Isaacs, 1981) suggests that later post-depositional degradation or migration of locally-deposited OC is likely negligible. OCMAR, the flux of OC buried in a sedimentary sequence, represents the combined effects of productivity, dilution, and preservation over time. Our new age model allows us to quantify changes in OCMAR through Monterey Formation sections, and directly compare the timing of OCMAR variability with the timing of putative regional and global drivers.

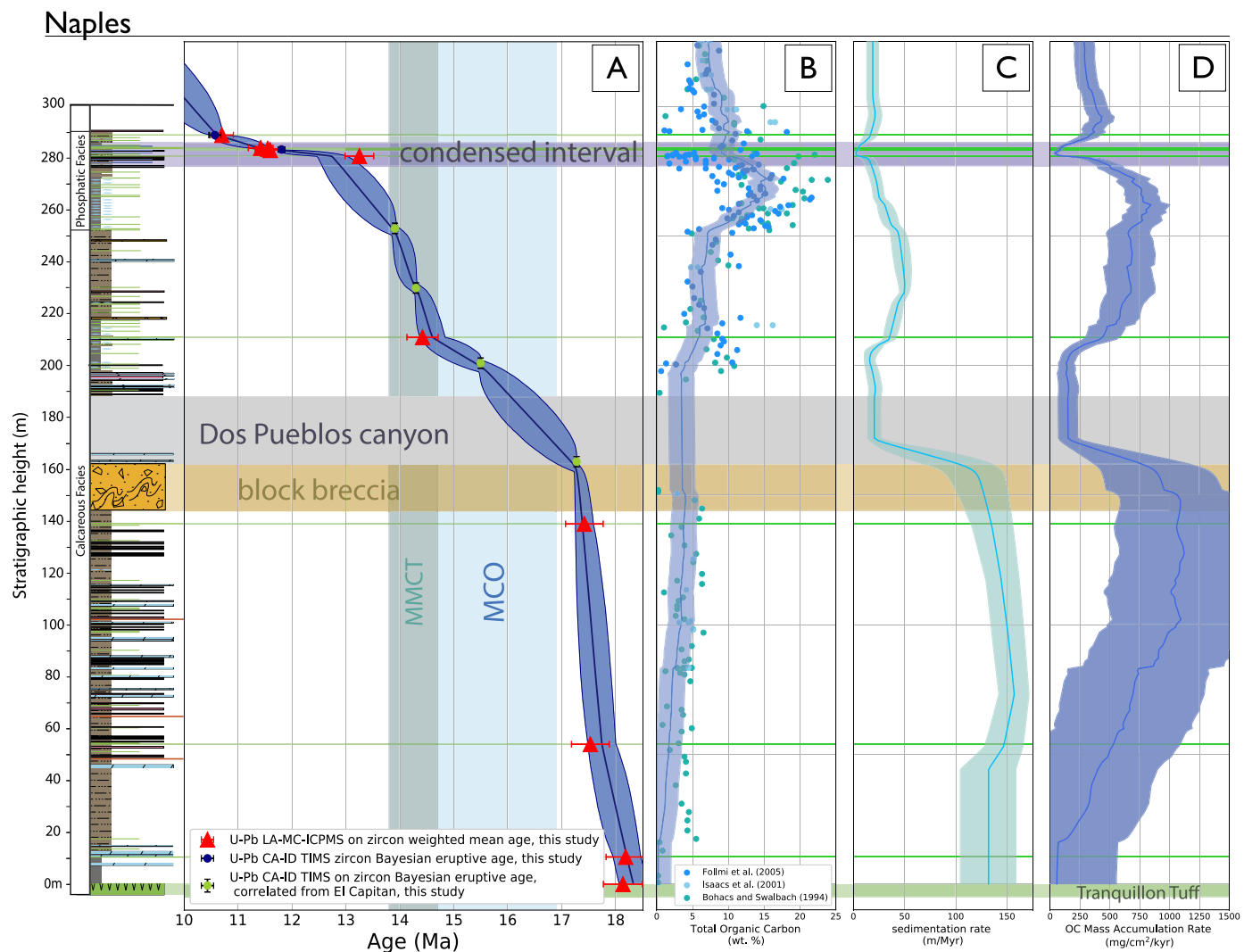


**Fig. 5.** Age model and modeled organic carbon mass accumulation rate (OCMAR) for Naples. A) age vs. height model for Naples, showing the 95% credible interval envelope of modeled age-height relationships. Note the usage of four ages correlated from the El Capitan section. The El Capitan ash ages were correlated to specific ash horizons at Naples Beach based on extant tephrochronological (Hornafius, 1994), biostratigraphic (John et al., 2002; Föllmi et al., 2005), and lithostratigraphic similarities between sections. However, they were incorporated into the age model with additional ( $\pm 1.5$  m) vertical uncertainty to account for potential miscorrelation. The temporal extents of the MCO and MMCT are represented by vertical bars. B) TOC data from Naples compiled from Föllmi et al. (2005), Isaacs et al. (2001), and Bohacs and Schwabach (1994), with a moving average through the data depicted as a solid line with  $1\sigma$  analytical uncertainty envelope. C) Modeled sedimentation rate for Naples with 68% credible interval envelope. D) Modeled OCMAR curve and 68% credible interval envelope for Naples, plotted vs. stratigraphic height.

The MCO and MMCT are defined by shifts in the  $\delta^{18}\text{O}$  composition of benthic foraminifera (Steinthorsdottir et al., 2021), which reflect a combination of seawater temperature and ice volume (Chappell and Shackleton, 1986). Peaks in OCMAR in the Monterey Formation occur prior to the onset of the MCO and during and after the MMCT (Fig. 6). These peaks could be interpreted to be consistent with the Monterey Hypothesis, as increased organic burial in Monterey strata is coincident with cooler intervals in the climatic proxy record (Fig. 6), potentially indicative of enhanced positive feedbacks between cooling, thermocline development, upwelling, and primary productivity (Vincent and Berger, 1985). Alternatively, OC burial in the Monterey Formation could be controlled by eustatically- and climatically-induced changes that extend beyond enhanced upwelling and productivity. These changes include shifts in regional hydrology (changing fluxes of nutrients or clay to the basin), basinal redox state (expansion/contraction of oxygen minima, changes in redox gradient depth), or basinal circulation (changing winnowing currents or upwelling), all of which can influence TOC abundance in Monterey Formation sediments.

Similarly, the coincidence between a drop in OCMAR and the onset of the MCO (Fig. 6) suggests a relationship, but the causality can again be interpreted in several ways: 1) warming or other climate-induced environmental changes could have caused a change in the magnitude or locus of upwelling and/or productivity, which could have driven a reduction in biogenous flux in the SBB during the MCO, or 2) sea-level rise could have caused changes in total sediment delivery to the borderland environment, which would manifest as reduced syn-MCO terrestrial flux to borderland depositional zones. These scenarios are considered within the context of a depositional model for the Monterey Formation in Section 5.3.

## 5.2. Relationships between sedimentation rate and TOC

Despite differences in the magnitude of both TOC content and sedimentation rate in contemporaneous intervals of the El Capitan (Fig. 4) and Naples (Fig. 5) sections, OCMAR at both localities is comparable in terms of both magnitude and variability (Fig. 6). Sedimentation rate and TOC abundance are inversely correlated at both locations ( $r$ -values of -0.67 and -0.44, respectively;

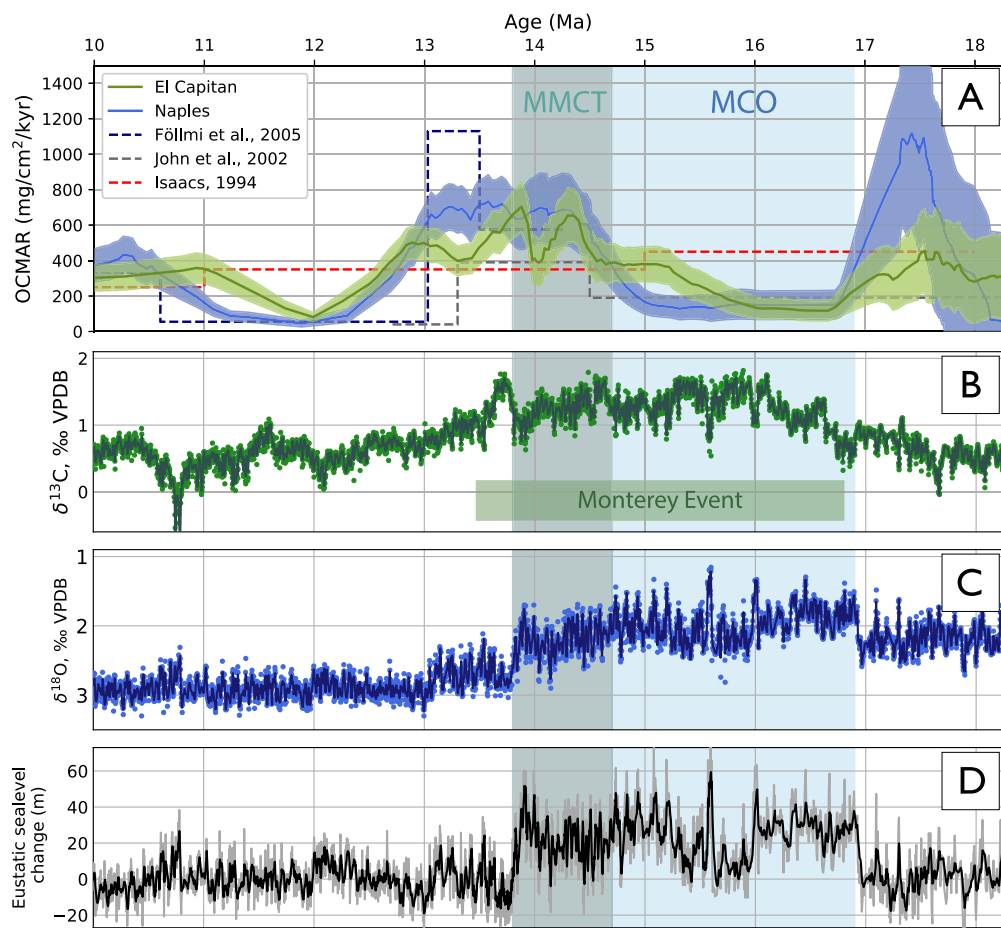


**Fig. 6.** A) Organic carbon mass accumulation rates (OCMARs) and 68% credible interval envelopes for El Capitan and Naples, plotted vs. time, with blue and teal intervals demarcating the temporal extent of the Miocene Climatic Optimum (MCO) and mid-Miocene Climatic Transition (MMCT) (Steinhorssdottir et al., 2021). Note relatively low OCMAR during the MCO. Previous estimates for OCMAR in the Santa Barbara Basin are shown as dashed lines. B) Compiled  $\delta^{13}\text{C}$  from benthic foraminiferal tests plotted vs. time (ODP cores 1337–1338, Westerhold et al., 2020), with the temporal extent of the Monterey Event positive  $\delta^{13}\text{C}$  isotope shift (Vincent and Berger, 1985) depicted as a green box. C) Compiled  $\delta^{18}\text{O}$  from benthic foraminifera plotted vs time (Westerhold et al., 2020). D) Modeled global eustatic sea level change, in meters (Miller, 2020).

Fig. 7A), yielding relatively low OCMARs in high-TOC intervals, and vice-versa, consistent with previous OCMAR estimates (John et al., 2002; Föllmi et al., 2005).

Secular differences in the relationships between TOC and various sediment component flux proxies observed in high- and low-sedimentation rate intervals at El Capitan (Fig. 7B-E) suggest that sedimentation rate influences processes that can control TOC abundance. Al/Si ratios, which serve as a proxy for clay abundance (Galy et al., 2007), are positively correlated with TOC, indicating the importance of clay shielding (Kennedy et al., 2002) as a preservation mechanism for TOC in the Miocene SBB. Furthermore, the slope of that positive correlation is dependent on sedimentation rate: lower sedimentation rates result in a much stronger relationship between clay and TOC than higher sedimentation rates, despite similar Al/Si ratios across all modeled sedimentation rates (Fig. 7B). This trend, which is also observed in Ti abundance (Fig. 7C), is consistent with the observed negative correlation between sedimentation rate and TOC abundance. At high sedimentation rates, dilution plays a dominant role in determining TOC abundance through the addition of material that either does not contain OC, or does not contribute to the preservation of organic material in the depozone. Conversely, at low sedimentation rates, strong relationships between clay proxies and TOC indicate the importance of preservation in determining TOC content. Indeed, the most linear relationship between TOC and clay abundance occurs during the post-MMCT interval at El Capitan (Fig. 7B), which features the lowest sedimentation rates observed in the section.

Relationships between TOC and biogenous flux proxies (Fig. 7D, E) are also dependent on sedimentation rate. Thus, as sedimentation rate affects a variety of factors that control the abundance of TOC, factors that control sedimentation rate were fundamental in determining the TOC content of Miocene Santa Barbara Basin strata. Importantly, in Holocene-to-modern Californian borderland basins, topographic variability and eustatic sea-level modulate sedimentation rates across the margin (Gorsline et al., 1968; Covault and Sharman, 2019).

### 5.3. Depositional model for organic carbon accumulation in the Santa Barbara Basin

With modern analogs in mind, we propose that a combination of local tectonics and eustasy were primary controls on Monterey Formation depositional systems, sedimentation rates, and organic carbon accumulation, with organic carbon deposition responding to, rather than driving, climatic variability. Changes in sea-level exacerbated the depositional effects of changing paleotopography in the tectonically evolving Miocene SBB, resulting in substantial changes in sedimentation rate and TOC abundance through both time and space (Fig. 8).

#### 5.3.1. Low sea level, high sedimentation rate

In this model, high sedimentation rates are most common during relative eustatic minima, when sediment sources (either terrigenous sources or banktops/shelves) are most likely to be

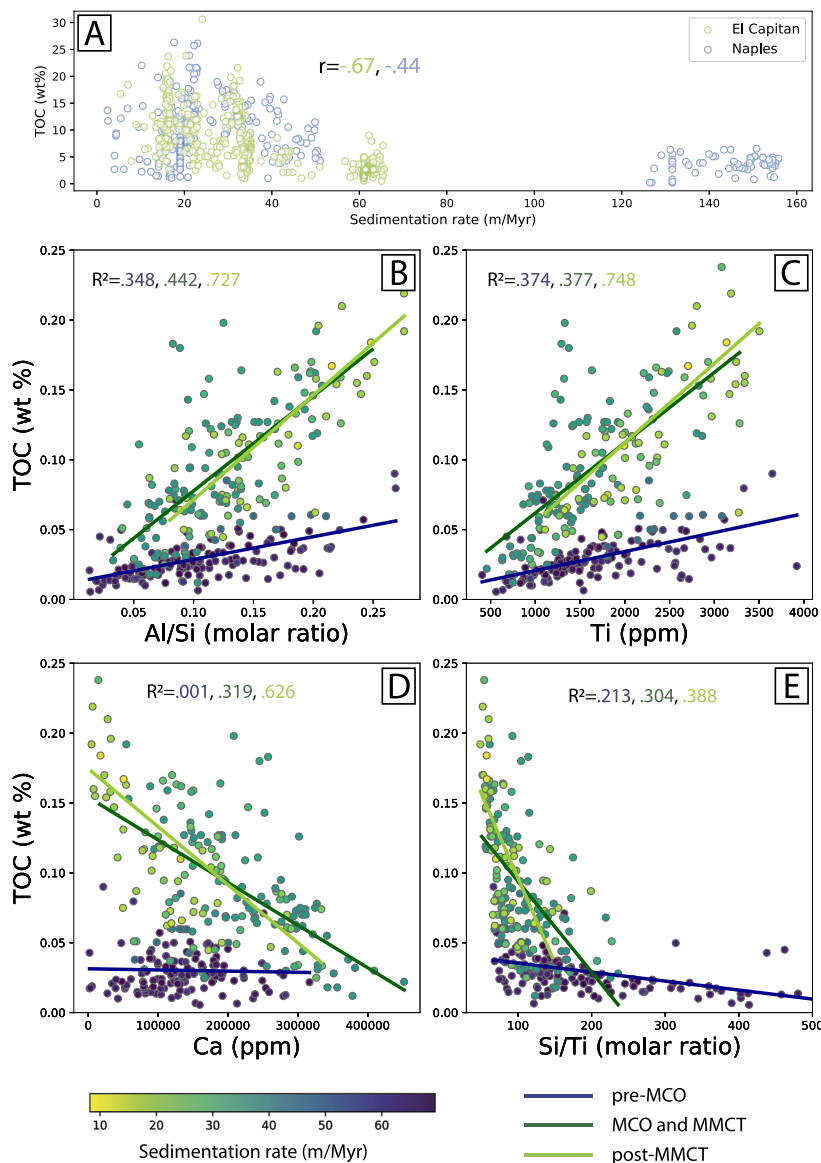


**Fig. 7.** A) Relationships between modeled sedimentation rate and TOC content at El Capitan and Naples, showing an inverse correlation at both localities ( $r$  values of -0.67 and -0.44, respectively). Comparison of TOC and elemental proxy data from El Capitan shales, including B) Al/Si ratio, a proxy for mineral surface area and clay abundance (Galy et al., 2007) plotted vs TOC. Higher Al/Si ratios generally indicate smaller grain size, more abundant clay, and a higher total mineral surface area. C) Ti abundance, a proxy for terrigenous flux variation (Rothwell and Croudace, 2015) with Ti increasing with increased terrigenous contributions, plotted vs TOC. D) Ca abundance and E) Si/Ti ratios, both proxies for biogenous vs terrigenous sediment flux changes (Rothwell and Croudace, 2015), plotted vs TOC. All data is shaded by modeled sedimentation rate at the sample height in the El Capitan section. Linear fits of the data for the pre-MCO, MCO+MMCT, and post-MMCT intervals are plotted to illustrate the importance of sedimentation rate in determining TOC abundance across different depositional regimes.

exposed to processes, such as gravitational instability, subaerial exposure, or current action, that mobilize and deposit sediment into available accommodation space (Fig. 8A). This is especially prevalent during periods of active faulting in the basin, during which time material accumulating on local topographic highs is frequently remobilized and redeposited into actively-generated accommodation space through mass-wasting processes. Shales (Fig. 8A), both massive and laminated, dominate intervals of the Miocene SBB with high post-compaction sedimentation rates. Although stepwise changes in terrigenous flux have been argued to be responsible for shifts in both sedimentation rate and OCMAR in the Miocene SBB (Isaacs, 1984), Monterey Formation shales contain a terrigenous component fraction that is consistently variable between ~20–60% throughout most of the Calcareous and Phosphatic Facies (Föllmi et al., 2005; Laurent et al., 2015), an interval which encompasses the full range of sedimentation rates modeled for

the SBB (Figs. 4,5). Similarly, Ti and Ca abundances express similar ranges of variability across a variety of sedimentation rates at El Capitan (Fig. 7C,D). This could be indicative of consistent, concomitant changes in independent biogenous and terrigenous fluxes to the depozone, yielding similar shale compositions at a variety of different sedimentation rates. Alternatively, shale deposition represents the remobilization of material previously deposited on shelves or banktops that is later distributed (purple arrows, Fig. 8) to depo-zones on the slope or shelf-slope transition, resulting in reworked, redeposited shales with compositions that reflect prior mixing of biogenous and terrigenous fluxes (blue and red arrows respectively, Fig. 8) in a shelf or banktop environment. This scenario agrees with the interpretations of Föllmi et al. (2005), who argue that most mudstones and shales observed at Naples Beach are the product of gravity-flow deposition, rather than vertical rain-out from distal suspended sediment load.

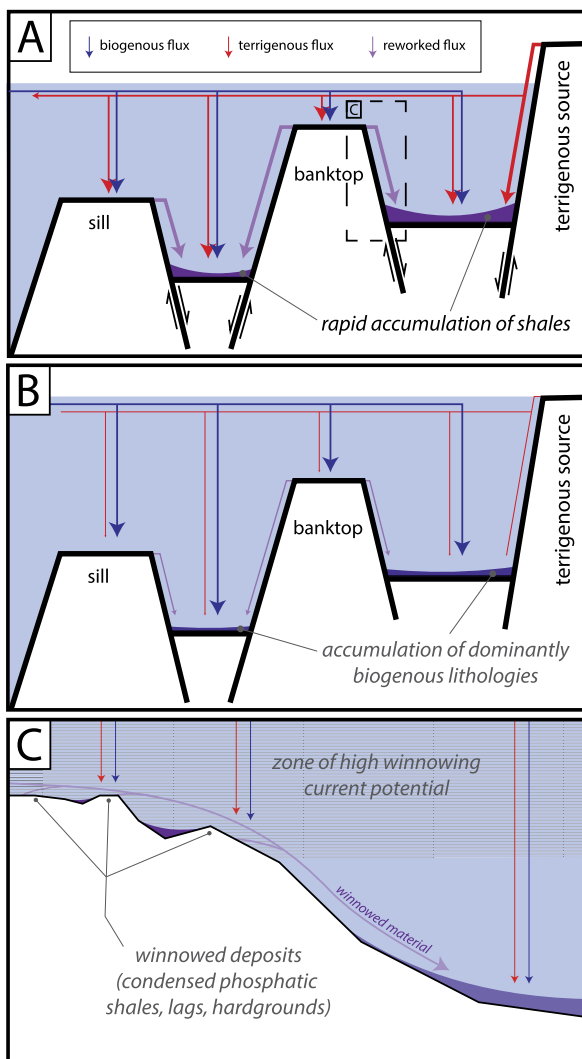


**Fig. 8.** Cartoon depiction of sedimentation patterns across the SBB, as controlled by tectonic and eustatic changes. Arrow sizes are proportional to flux magnitude. A) Low sea level and active tectonism result in the deposition of both primary and remobilized sediment into newly created accommodation space. High sedimentation rates, dominated by remobilized sediment flux, result in thick shales with relatively low TOC content. Dashed box shows area detailed in panel C. B) High sea level reduces terrigenous flux to the depozone, as well as diminishes the ability of shallow current action to rework material on submerged paleotopographic highs. Biogenous flux becomes the dominant sediment source, resulting in deposition of biogenous lithologies. C) Detail of a submerged paleotopographic high, illustrating topographic control on thickness and lithologic variability.

The highest sedimentation rates and lowest sustained TOC concentrations observed in this study are hosted within the pre-MCO basal Monterey Formation, which is dominated by shale lithologies (Fig. 2A). The elevated sedimentation rates through this interval drive relationships between TOC and proxies for clay, terrigenous sediment abundance, and biogenous sediment abundance that are distinct from those in younger intervals with lower, albeit more variable sedimentation rates (Fig. 7). Importantly, this interval contains abundant evidence of active tectonism and basinal evolution: large thickness differences between sections (Fig. 1) suggest variable generation of accommodation space likely related to normal faulting on the interior margin of the basin along present day Santa Cruz Island (Hornafius, 1991), culminating with the deposition of slumped block breccias (Fig. 2F) found across the SBB at ~17.0 Ma (Fig. 1). It is unclear whether the block breccia horizon represents a single event (e.g., a seismite) or is the result of tectonically- or eustatically-induced instability. While debris flows

occur along the modern Californian margin during intervals of both sea-level rise and fall, debris flows that occurred during transgressions are most common (Covault and Graham, 2010). The temporal proximity of the onset of the MCO with the block breccia horizon suggests a potential association with the transgression at the onset of the MCO. Furthermore, the occurrence of a coarse litharenitic sandstone within the breccia horizon at the El Capitan locality is indicative of the presence of a likely-proximal terrigenous sediment source to the Miocene SBB. However, similar to the modern Californian margin, the throughflow of coarse clastic material to basinal depozones may have been largely restricted to submarine canyons (Covault and Sharman, 2019), resulting in the observed dearth of coarse clastic material in the northern SBB outcrops.

### 5.3.2. High sea level, low sedimentation rate

During relative sea level maxima, potential sediment sources are inundated, resulting in a reduction of both terrigenous material and remobilized banktop material to the depozone (Fig. 8B). Biogenous material becomes the most voluminous contribution to the depozone, resulting in the accumulation of dominantly biogenous lithologies.

This model scenario is best represented in the SBB by a decrease in apparent sedimentation rate at ~17.0 Ma that is concomitant with a shift in dominant lithology from calcareous shale to porcelainite beds (Fig. 1; Fig. 2B), as well as low-to-moderate TOC and a decrease in OCMAR. The base of this interval aligns temporally with the onset of the MCO (Herbert et al., 2022; Westerhold et al., 2020) and a eustatic sea-level rise at ~16.9 Ma of ~40 m (Miller et al., 2020). This scenario supports previously proposed models for the occurrence of biogenous lithologies as the result of reduced detrital input (Isaacs, 1984), and suggests that reduced terrigenous input, rather than a reduction in primary productivity, is responsible for reduced OCMAR across the early MCO interval. Additionally, the low TOC measured through this interval can potentially be explained by the reduction of detrital material to the depozone, thereby limiting clay-mediated preservation of TOC and resulting in concomitant local minima in sedimentation rate and TOC abundance that are not observed elsewhere in the section. Alternatively, the high porosity and permeability of dominantly biogenous material in a pre-compaction setting could have resulted in the relatively poor preservation of OC, driving both low TOC and low post-compaction apparent sedimentation rate.

### 5.3.3. Low sea level, low sedimentation rate

When material is transferred from relatively high topography (e.g. sills or banktops, Fig. 8) into adjacent accommodation space, highly condensed stratigraphy and/or unconformities will develop along those topographic highs (Fig. 8C). During periods of rapid uplift or topographic generation, gravitational mass wasting will remobilize most material found on banktops, regardless of grain-size, density or hydraulic stability. When the dominant source of sediment remobilization is current action, however, material above a certain grain size, density, or hydraulic stability threshold will remain in-situ, while more easily-mobilized material is scoured and redeposited elsewhere. As a result, lowstand intervals during which banktops, shelves, and slopes are exposed to persistent winnowing currents will feature condensed regions with extremely low sedimentation rates and a high probability of significant unconformity surfaces.

This scenario is exemplified in the SBB by rocks of the Phosphatic Facies (Fig. 1), which host both the lowest sedimentation rates and highest TOC contents measured in the basin. A ~60 m sea-level fall associated with East Antarctic Ice Sheet (EAIS) growth beginning at ~13.8 Ma (Holbourn et al., 2014; Miller et al., 2020) may have amplified paleotopographic variability across banktop highs (Hornafius, 1991) in the northern SBB. This variability drove

the deposition of discontinuous lag deposits of reworked authigenic phosphatic nodules and phosphatic hardgrounds (Fig. 2C), which define the condensed interval of the Phosphatic facies. Differences in condensation between sections are significant, resulting in this interval containing the only long-lived decoupling of OCMARs between El Capitan and Naples beaches (Fig. 6). At El Capitan and Naples, the condensed interval spans 13.25 Ma to just younger than 11.32 Ma, while hardgrounds appear before 14.27 Ma at Tajiguas Beach, and are abundant between 13.89 Ma and 10.15 Ma (Fig. 1). The Phosphatic Facies contains evidence of sediment reworking (Fig. 2D) and variable hydrodynamic conditions across sub-decimeter lateral distances, with authigenic calcareous and phosphatic material forming clast-supported conglomeratic lags in regions where finer material has been winnowed away (Fig. 2C).

A strong positive relationship between Al/Si ratio and TOC through this interval (Fig. 7A) suggests that even in a winnowing environment, clay abundance plays a significant role in determining the abundance of organic carbon. While this may seem counterintuitive for an environment wherein fine-grained material is preferentially removed, both directional currents and waves can concentrate clays in the shallow subsurface of the sediment, resulting in a clay-enriched layer that is more resistant to hydraulic removal than adjacent, clay-poor horizons (Wu et al., 2018). The development of an “armored” clay-rich layer provides a mechanism for maintaining clays in an actively-winnowing environment, and also provides an avenue for porosity reduction in the upper sediment column. Föllmi et al. (2005) argue that porosity reduction during phosphogenesis provides enhanced preservational potential for OC by limiting porewater throughput and decreasing oxidative remineralization potential below low-porosity horizons. The exceptional TOC content (and resultant variable OCMAR) of the post MMCT interval may therefore be a function of preservation both by clay shielding as well as by porosity reduction associated with both winnowing-related clay armoring and phosphogenesis, with the locus of winnowing and phosphogenesis controlled by basinal topography (Föllmi et al., 2005, 2017).

#### 5.4. Timing and magnitude of organic carbon accumulation in the Monterey Formation

The age model presented here demonstrates that these TOC-rich sections along the SBB coast that were used to argue for increased organic burial during the MCO and MMCT (Flower and Kennett, 1993) have moderate OCMARs because they are condensed. This does not necessarily imply that all Monterey Formation exposures that formed in other settings will have the same record of organic burial, as different depositional systems will respond differently to sea-level change. For example, during lowstands, when upper slope and banktop sections are winnowed, more fine material, including clay, may be delivered to deeper-water sections, promoting enhanced carbon burial (Fig. 8A). Indeed, seismic profiles across the Santa Barbara channel suggest significant thickening of units contemporaneous with the condensed interval of the northern SBB Phosphatic Facies (Hornafius, 1991). Thus, for the Monterey Hypothesis to be retained, exceptional organic carbon burial would have had to have occurred elsewhere on the California margin, away from the northern SBB sections in offboard deposits.

Exceptional rates of organic carbon burial are not the baseline in the Miocene SBB: the maximum OCMAR observed at Naples Beach, which precedes the MCO, is within the range of OCMARs measured along Holocene productive margins (Fig. 9). In general, SBB strata host OCMARs more akin to those observed on lower productivity margins or within the modern California borderland basins (between ~250–1650 mg/cm<sup>2</sup>/kyr, Jahnke, 1990). Estimated OCMARs from the Belridge Field of the San Joaquin

Basin, an expanded, clastic-rich Monterey Formation locality, are similar to those of the SBB sections and modern Californian borderland basins (Fig. 9), ranging between ~490–2200 g/cm<sup>2</sup>/kyr (see Supplementary Materials). However, the current age model for Belridge Field strata (Scheirer and Magoon, 2007) suggests that the highest OCMARs in this interval postdate the end of the MMCT, undermining arguments for a driving relationship between OC burial in the Monterey Formation and the onset of Miocene cooling.

#### 5.5. Organic burial in the Monterey Formation and the Monterey Event

A core tenet of the Monterey Hypothesis is the proposed correlation between positively-shifted  $\delta^{13}\text{C}$  values of the Monterey Event with enhanced episodes of organic burial in the Monterey Formation (Vincent and Berger, 1985; Flower and Kennett, 1993). The Monterey Event is characterized by a +1‰ shift in the  $\delta^{13}\text{C}$  of foraminiferal tests (interpreted to record changes in the isotopic composition of marine dissolved inorganic carbon, or DIC) from marine sediment cores around the globe. The  $\delta^{13}\text{C}$  of DIC is set by the sum of the isotopic composition and fluxes of inputs and outputs of carbon into the global marine reservoir, and can be schematically represented with a simple single-box model (Fig. 10A). On timescales longer than the residence time of carbon in the deep ocean, this model can be simplified by assuming a steady state, with the magnitude and composition of output fluxes balancing those of the input (Kump and Arthur, 1999):

$$\delta^{13}\text{C}_{\text{in}} = (\delta^{13}\text{C}_{\text{org}} \times f_{\text{org}}) + \delta^{13}\text{C}_{\text{carb}} \times (1 - f_{\text{org}}) \quad (3)$$

Here,  $f_{\text{org}}$  represents the fraction of carbon that is removed from the marine reservoir as organic carbon, while  $\delta^{13}\text{C}_{\text{in}}$ ,  $\delta^{13}\text{C}_{\text{org}}$ , and  $\delta^{13}\text{C}_{\text{carb}}$  represent the isotopic compositions of carbon input into the marine system, buried organic carbon, and carbon in buried carbonates, respectively. Although this relationship is an oversimplification of the dynamic global carbon cycle, this mass balance model provides a quantitative test of hypotheses related to changes in organic carbon burial. Here, we use this framework to assess the significance of the rates of organic carbon burial in the Monterey Formation relative to the mass-balance requirements of the ~1‰  $\delta^{13}\text{C}$  excursion of the Monterey Event.

Assuming an input isotopic composition of -6‰ (roughly the composition of volcanic CO<sub>2</sub>; Shields and Mills, 2017) and an average  $\delta^{13}\text{C}_{\text{org}}$  composition of -23‰, which approximates the average  $\delta^{13}\text{C}$  of global Miocene organic carbon (Katz et al., 2005) as well as  $\delta^{13}\text{C}_{\text{org}}$  of the Monterey Formation (mean  $\delta^{13}\text{C}_{\text{org}}$  of -23.18‰ in El Capitan shales, Table SM4; Laurent et al., 2015) the ~1‰ shift in the  $\delta^{13}\text{C}$  of DIC observed during the Monterey Event could have been driven by an increase in  $f_{\text{org}}$  of ~10% (from 0.277 to 0.306), with no appreciable change in total C flux in or out of the global surface system. Given an assumed conservative average global carbon burial flux of ~0.6 GtC/yr (Li et al., 2023), this shift in  $f_{\text{org}}$  requires an additional 0.017 GtC/yr flux of organic carbon out of the marine system. If all this additional flux was accommodated by organic burial in the Monterey Formation (assuming a depositional area of ~180,000 km<sup>2</sup>, equivalent to the total area of Neogene basins outlined in Fig. 1A), an OCMAR of 9,440 mg/cm<sup>2</sup>/kyr would need to have been sustained across all Californian Neogene basins during Monterey Event time. Expanding depositional area to an estimate of total circum-Pacific Neogene basin area (~600,000 km<sup>2</sup>; Vincent and Berger, 1985) yields a sustained OCMAR of 2833 mg/cm<sup>2</sup>/kyr. This rate is higher than those reported anywhere in the Monterey Formation, and substantially higher than those observed in the SBB during early Monterey Event time (<250 mg/cm<sup>2</sup>/kyr from 15.75–16.75 Ma, Fig. 6). A simple sensitivity test (see Supplementary Materials) shows that this relationship is replicated by a range of reasonable estimated  $\delta^{13}\text{C}_{\text{in}}$

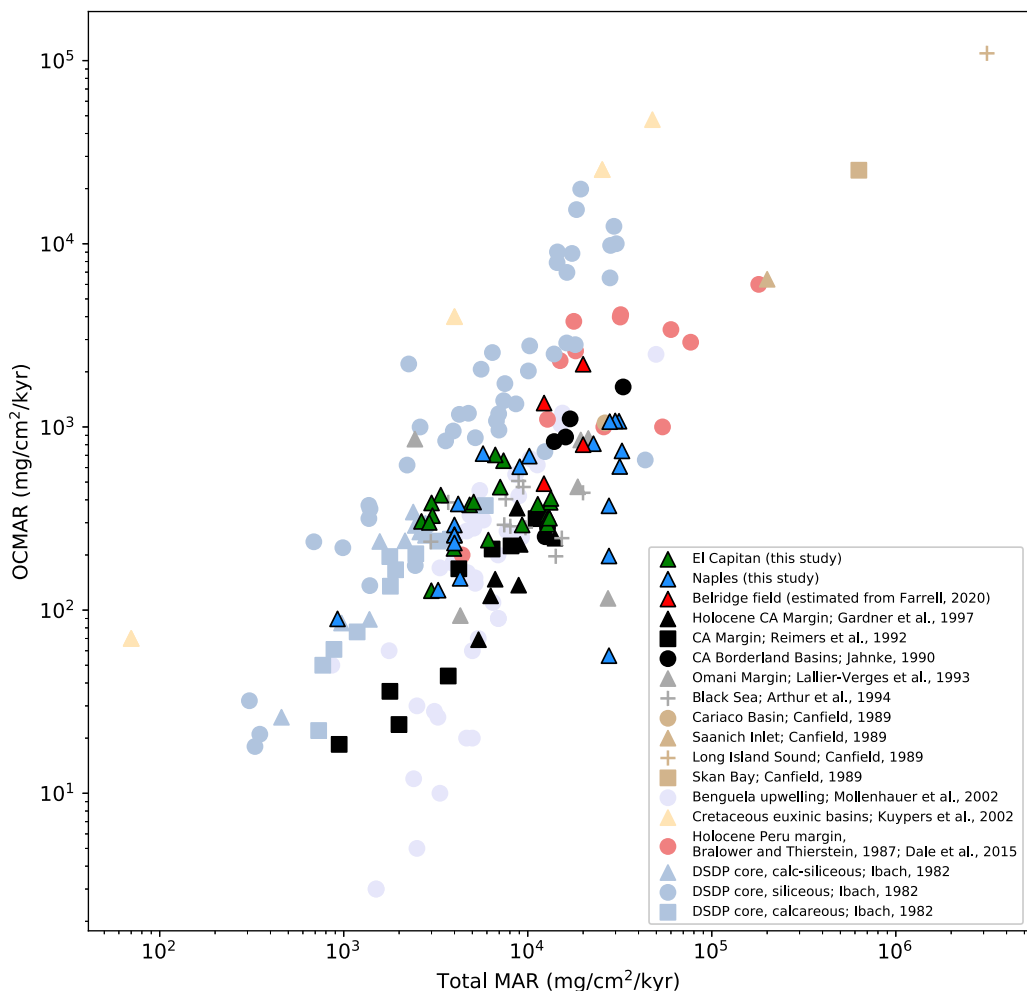


**Fig. 9.** Ranges of OCMAR from El Capitan and Naples, as well as estimated OCMARs from the Belridge oil field of the San Joaquin Valley, plotted against total mass accumulation rate (MAR). Note log scale. Also included are OCMAR vs total MAR for a variety of different localities, including the Californian Margin (Gardner et al., 1997; Reimers et al., 1992), California Borderland Basins (Jahnke, 1990), the Omani Margin (Lallier-Verges et al., 1993), the Black Sea (Arthur et al., 1994), the Cariaco Basin, Saanich Inlet, Long Island Sound, and Skan Bay (Canfield, 1989), the southwestern African margin (Mollenhauer et al., 2002), Cretaceous euxinic basins (Kuypers et al., 2002), the Holocene Peruvian margin (Bralower and Thierstein, 1987; Dale et al., 2015), and data compiled from various Deep Sea Drilling Project (DSDP) cores (Ibach, 1982). Figure adapted from Gardner et al., 1997. Note the overlap of calculated Monterey Formation OCMAR ranges with typical values from the modern California margin and Borderland Basins.

and  $\delta^{13}\text{C}_{\text{org}}$  values. It is therefore unlikely that organic burial in the Monterey Formation, or indeed in all circum-Pacific basins, was the primary driver of the positive isotopic excursion of the Monterey Event.

#### 5.6. Alternative drivers of the Monterey Event

Similar to the Monterey Formation, global rates of organic carbon burial may have responded to, rather than driven, changes in global climate. The positively-shifted foraminiferal  $\delta^{13}\text{C}$  values of the Monterey Event begin during the MCO, and lag an abrupt shift in foraminiferal  $\delta^{18}\text{O}$  values (Fig. 6) associated with warming, ice loss, and sea-level rise at the beginning of the MCO (Hobbs et al., 2014). Eustatic sea level models suggest a ~40 m syn-MCO transgression (Miller et al., 2020), providing support for hypotheses that propose enhanced organic carbon burial on continental shelves during eustatic maxima (Fig. 10B) as a driver of positive marine  $\delta^{13}\text{C}$  excursions (Compton et al., 1990; Bjerrum et al., 2006; Sosdian et al., 2020). Inundation of continental shelves may have produced an increase in shallow marine depositional environments that can support more efficient organic burial than the deep ocean (Hedges and Keil, 1995). This hypothesis is supported by the mid-Miocene geological record: estuarine coals on

the Sunda Shelf record evidence of enhanced organic carbon deposition in nearshore marginal environments (Fikri et al., 2022), while phosphorites on the eastern seaboard of North America have been interpreted as the product of organic-rich deposits that were emplaced during syn-MCO highstands and subsequently oxidized during lowstands (Compton et al., 1990).

This hypothesis is distinct from that of Li et al. (2023), who present a global compilation of Neogene organic carbon burial rates in deep marine environments, and argue that a decrease in marine organic burial during the Middle Miocene is indicative of low global organic carbon burial rates and anemic global  $f_{\text{org}}$ . However, the locations that make up this compilation largely sample open marine depositional environments that represent a small fraction of global organic burial (Hedges and Keil, 1995). Thus, the organic carbon burial record of Li et al. (2023), and indeed in the Monterey Formation, could be interpreted as a syn-MCO fractional shift in the locus of marine primary productivity, export, and burial from deeper marine environments to shallower, marginal environments associated with changes in sea level. The apparent decrease in deep marine OC burial would therefore be compensated by the increased burial and/or recycling of organic carbon in proximal environments, consistent with the shelf-inundation hypotheses discussed above.

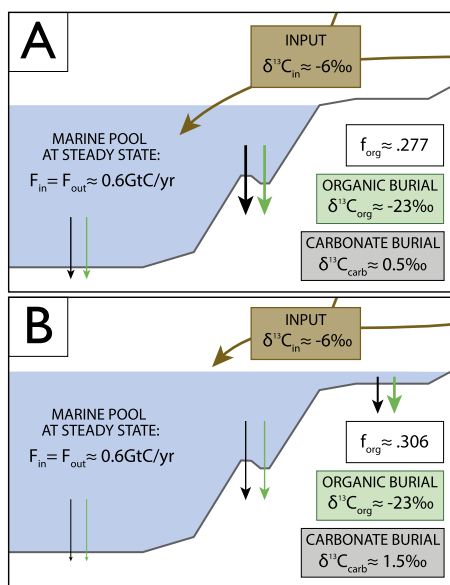


**Fig. 10.** Cartoon depiction of a simple box model describing the isotopic mass balance required to set the  $\delta^{13}\text{C}$  of the marine dissolved inorganic carbon (DIC) pool. Both panels represent steady state conditions, with  $F_{in}$  (total flux of carbon input into the marine pool from all sources) set equal to  $F_{out}$  (total flux of carbon output from the marine pool, which is the sum of organic burial and carbonate burial fluxes). Input/output flux is assumed to be  $\sim 0.6\text{GtC/yr}$ . Panel A) represents a pre-Monterey Event scenario with carbonate burial ( $\delta^{13}\text{C}_{carb}$ ) isotopic compositions of  $\sim 0.5\text{\textperthousand}$ , requiring a ratio of organic to carbonate burial ( $f_{org}$ ) of  $\sim 0.277$ . B) represents a syn-Monterey Event scenario, in which  $\delta^{13}\text{C}_{carb}$  is driven to  $\sim 1.5\text{\textperthousand}$  by an increase in  $f_{org}$  to  $\sim 0.306$ . We suggest that some of the implied increase in organic carbon burial was accommodated by burial in proximal, supra-shelf environments during the syn-MCO transgression. In both panels, the scale of the black (carbonate) and green (organic) arrows schematically represents the relative magnitude of carbon burial in deep marine (left), distal marginal (center) and proximal/supra-shelf (right) environments. Note that during the MCO, a relocation of a fraction of organic burial to newly-inundated epicontinentally settings may have balanced decreases in deep marine organic burial rates, consistent with the observations of Li et al. (2023).

## 5.7. Organic carbon burial and Miocene climate

Although organic carbon burial in the Monterey Fm and equivalent circum-Pacific basinal deposits cannot explain the Monterey Event alone, the isotopic shift of the Monterey Event may have been related to transgression and organic carbon burial over a broader continental shelf area, and can be achieved without changing the total global carbon burial flux. In this scenario, changes in the inorganic carbon cycle must be invoked to exert influence on global carbon mass balance and drive climate change, to which a dynamic organic carbon cycle would then respond. Potential inorganic drivers of the MCO warming include the outgassing of  $\text{CO}_2$  associated with the eruption of the Columbia River Flood Basalts, with weathering of the resultant basaltic edifice contributing to subsequent cooling (Hodell and Woodruff, 1994) for several million years after the cessation of volcanism at ca. 15.9 Ma (Kasbohm and Schoene, 2018). Additional changes in inorganic carbon sources from slowing seafloor spreading rates (Herbert et al., 2022) or changes in sinks from enhanced silicate weathering in the tropics (Park et al., 2020) have been proposed as contributors to Miocene cooling. Our data from the Monterey Formation are consistent with hypotheses for inorganic geological drivers of long-term climate change, and support the notion that organic carbon burial in the Miocene responded to, rather than drove, global climate.

## 6. Conclusions

A new age model for the Monterey Formation incorporates 31 new LA-ICPMS and 14 CA-ID-TIMS U-Pb zircon ages from the

northern coast of the Santa Barbara Channel. Modeled sedimentation rates from this age model were combined with TOC data from sections at El Capitan and Naples to assess the magnitude and timing of OCMAR in the Miocene Santa Barbara Basin, and show that peaks in SBB OCMAR do not correspond with the Monterey Event shift in the global  $\delta^{13}\text{C}_{\text{DIC}}$  record from a timing or mass-balance perspective. Rather than driving climate, TOC burial in the Monterey Formation was controlled by changes in sedimentation rate, which was in turn controlled by a combination of local tectonics and eustasy. Thus, contrary to the driving relationship postulated by the Monterey Hypothesis, organic carbon deposition in the Monterey Formation was largely a response to basin formation and climate change.

## CRediT authorship contribution statement

**Eliel S.C. Anttila:** Writing – review & editing, Writing – original draft, Visualization, Validation, Software, Resources, Methodology, Investigation, Funding acquisition, Formal analysis, Data curation, Conceptualization. **Francis A. Macdonald:** Writing – review & editing, Validation, Supervision, Project administration, Methodology, Investigation, Funding acquisition, Conceptualization. **Dawid Szymanowski:** Writing – review & editing, Validation, Formal analysis, Data curation. **Blair Schoene:** Writing – review & editing, Validation, Supervision, Resources, Methodology, Formal analysis, Data curation. **Andrew Kylander-Clark:** Resources, Methodology, Formal analysis, Data curation. **Clara Danhof:** Methodology, Formal analysis, Data curation. **David S. Jones:** Writing – review & editing, Validation, Resources, Methodology, Investigation, Formal analysis, Data curation.

## Declaration of competing interest

The authors declare that they have no known competing financial interests or personal relationships that could have appeared to influence the work reported in this paper.

## Data availability

Data presented in this publication are available in the following repository: [https://github.com/eliel-anttila/Anttila\\_Monterey\\_2023](https://github.com/eliel-anttila/Anttila_Monterey_2023).

## Acknowledgements

This project was funded by American Chemical Society (ACS) PRF #65256-ND8 to FAM. ESCA was additionally supported by National Science Foundation (NSF) Graduate Research Fellowship Program (GRFP) 2139319 and NSF Frontier Research in Earth Science (FRES) Grant FRES1925990 to FAM. We thank Scott Hornafius and Jim Boles for stimulating conversations and constructive feedback, and thank Caroline Newell and Brian Mo for their assistance with sample preparation.

## Appendix A. Supplementary material

Supplementary material related to this article can be found online at <https://doi.org/10.1016/j.epsl.2023.118343>.

## References

- Agnihotri, R., Altabet, M.A., Herbert, T.D., Tierney, J.E., 2008. Subdecadally resolved paleoceanography of the Peru margin during the last two millennia. *Geochim. Geophys. Geosyst.* 9 (5). <https://doi.org/10.1029/2007GC001744>.
- Arthur, M.A., Dean, W.E., Neff, E.D., Hay, B.J., King, J., Jones, G., 1994. Varve calibrated records of carbonate and organic carbon accumulation over the last 2000 years in the Black Sea. *Glob. Biogeochem. Cycles* 8 (2), 195–217. <https://doi.org/10.1029/94GB00297>.

- Barron, J.A., 1986. Paleoceanographic and tectonic controls on deposition of the Monterey Formation and related siliceous rocks in California. *Palaeogeogr. Palaeoclimatol. Palaeoecol.* 53 (1), 27–45. [https://doi.org/10.1016/0031-0182\(86\)90037-4](https://doi.org/10.1016/0031-0182(86)90037-4).
- Behl, R.J., Moores, E.M., Sloan, D., Stout, D.L., 1999. Since Bramlette (1946): the Miocene Monterey Formation of California revisited: Classic Cordilleran Concepts: a View from California. *Spec. Pap., Geol. Soc. Am.*, vol. 338, pp. 301–313.
- Blättler, C.L., Miller, N.R., Higgins, J.A., 2015. Mg and Ca isotope signatures of authigenic dolomite in siliceous deep-sea sediments. *Earth Planet. Sci. Lett.* 419, 32–42. <https://doi.org/10.1016/j.epsl.2015.03.006>.
- Bjerrum, C.J., Bendtsen, J., Legarth, J.J.F., 2006. Modeling organic carbon burial during sea level rise with reference to the Cretaceous. *Geochem. Geophys. Geosyst.* 7 (5). <https://doi.org/10.1029/2005GC001032>.
- Bohacs, K.M., Schwalbach, J.R., 1994. Natural gamma-ray spectrometry of the Monterey Formation at Naples Beach, California: insights into lithology, stratigraphy, and source-rock quality. In: *Field Guide to the Monterey Formation Between Santa Barbara and Gaviota*. AAPG Pacific Section, California, pp. 85–94.
- Bralower, T.J., Thierstein, H.R., 1987. Organic carbon and metal accumulation rates in Holocene and mid-Cretaceous sediments: palaeoceanographic significance. *Geol. Soc. (Lond.) Spec. Publ.* 26 (1), 345–369. <https://doi.org/10.1144/GSL.SP.1987.026.01.23>.
- Bramlette, M.N., 1946. *The Monterey Formation of California and the Origin of Its Siliceous Rocks*, vol. 212. US Government Printing Office, Washington D.C. 57 p.
- Calvert, S.E., Pedersen, T.F., 2007. Chapter fourteen elemental proxies for palaeoclimatic and palaeoceanographic variability in marine sediments: interpretation and application. *Dev. Mar. Geol.* 1, 567–644. [https://doi.org/10.1016/S1572-5480\(07\)01019-6](https://doi.org/10.1016/S1572-5480(07)01019-6).
- Canfield, D.E., 1989. Sulfate reduction and oxic respiration in marine sediments: implications for organic carbon preservation in euxinic environments. *Deep-Sea Res., A, Oceanogr. Res. Pap.* 36 (1), 121–138. [https://doi.org/10.1016/0198-0149\(89\)90022-8](https://doi.org/10.1016/0198-0149(89)90022-8).
- Chappell, J., Shackleton, N., 1986. Oxygen isotopes and sea level. *Nature* 324 (6093), 137–140. <https://doi.org/10.1038/324137a0>.
- Compton, J.S., Snyder, S.W., Hodell, D.A., 1990. Phosphogenesis and weathering of shelf sediments from the southeastern United States: implications for Miocene  $^{81}\text{C}$  excursions and global cooling. *Geology* 18 (12), 1227–1230.
- Covault, J.A., Graham, S.A., 2010. Submarine fans at all sea-level stands: tectono-morphologic and climatic controls on terrigenous sediment delivery to the deep sea. *Geology* 38 (10), 939–942. <https://doi.org/10.1130/G31081.1>.
- Covault, J.A., Sharman, G.R., 2019. Tectonostratigraphic evolution of the inner California borderland: template for fill-and-spill sedimentation. In: *The Sedimentary Basins of the United States and Canada*. Elsevier, pp. 511–528.
- Crouch, J.K., Bukry, D., 1979. Comparison of Miocene provincial foraminiferal stages to coccolith zones in the California continental borderland. *Geology* 7 (4), 211–215. [https://doi.org/10.1130/0091-7613\(1979\)7<211:COMPFS>2.0.CO;2](https://doi.org/10.1130/0091-7613(1979)7<211:COMPFS>2.0.CO;2).
- Dale, A.W., Sommer, S., Lomnitz, U., Montes, I., Treude, T., Liebetrau, V., Gier, J., Hensen, C., Dengler, M., Stolpovsky, K., Bryant, L.D., 2015. Organic carbon production, mineralisation and preservation on the Peruvian margin. *Biogeosciences* 12 (5), 1537–1559. <https://doi.org/10.5194/bg-12-1537-2015>.
- Fenton, N.C., 2018. *Zircon U-Pb Dating of Tuff in the Monterey Formation of California by Laser Ablation Inductively Coupled Plasma Mass Spectrometry*. Doctoral dissertation. San Diego State University, 99 p.
- Fikri, H.N., Sachsenhofer, R.F., Bechtel, A., Gross, D., 2022. Organic geochemistry and petrography in Miocene coals in the Barito Basin (Tutupan Mine, Indonesia): evidence for astronomic forcing in kerapah type peats. *Int. J. Coal Geol.* 256, 103997. <https://doi.org/10.1016/j.jcoal.2022.103997>.
- Flower, B.P., Kennett, J.P., 1993. Relations between Monterey Formation deposition and middle Miocene global cooling: Naples Beach section, California. *Geology* 21 (10), 877–880. [https://doi.org/10.1130/0091-7613\(1993\)021<0877:RBMFDA>2.3.CO;2](https://doi.org/10.1130/0091-7613(1993)021<0877:RBMFDA>2.3.CO;2).
- Föllmi, K.B., Badertscher, C., de Kaenel, E., Stille, P., John, C.M., Adatte, T., Steinmann, P., 2005. Phosphogenesis and organic-carbon preservation in the Miocene Monterey Formation at Naples Beach, California—The Monterey hypothesis revisited. *Geol. Soc. Am. Bull.* 117 (5–6), 589–619.
- Föllmi, K.B., Thomet, P., Lévy, S., De Kaenel, E., Spangenberg, J.E., Adatte, T., Behl, R.J., Garrison, R.E., 2017. The impact of hydrodynamics, authigenesis, and basin morphology on sediment accumulation in an upwelling environment: the Miocene Monterey Formation at Shell Beach and Mossel Rock (Pismo and Santa Maria Basins, Central California, USA). *J. Sediment. Res.* 87 (9), 986–1018. <https://doi.org/10.2110/jsr.2017.57>.
- Foster, G.L., Lear, C.H., Rae, J.W., 2012. The evolution of  $\text{pCO}_2$ , ice volume and climate during the middle Miocene. *Earth Planet. Sci. Lett.* 341, 243–254. <https://doi.org/10.1016/j.epsl.2012.06.007>.
- Galy, V., France-Lanord, C., Beyssac, O., Faure, P., Kudrass, H., Palhol, F., 2007. Efficient organic carbon burial in the Bengal fan sustained by the Himalayan erosional system. *Nature* 450 (7168), 407–410. <https://doi.org/10.1038/nature06273>.
- Gardner, J.V., Dean, W.E., Dartnell, P., 1997. Biogenic sedimentation beneath the California current system for the past 30 kyr and its paleoceanographic significance. *Paleoceanography* 12 (2), 207–225. <https://doi.org/10.1029/96PA03567>.
- Gorsline, D.S., Drake, D.E., Barnes, P.W., 1968. Holocene sedimentation in Tanner Basin, California continental borderland. *Geol. Soc. Am. Bull.* 79 (6), 659–674. [https://doi.org/10.1130/0016-7606\(1968\)79\[659:HSITBC\]2.0.CO;2](https://doi.org/10.1130/0016-7606(1968)79[659:HSITBC]2.0.CO;2).
- Hancock, L.G., Hardisty, D.S., Behl, R.J., Lyons, T.W., 2019. A multi-basin redox reconstruction for the Miocene Monterey Formation, California, USA. *Palaeogeogr. Palaeoclimatol. Palaeoecol.* 520, 114–127. <https://doi.org/10.1016/j.palaeo.2019.01.031>.
- Hedges, J.I., Keil, R.G., 1995. Sedimentary organic matter preservation: an assessment and speculative synthesis. *Mar. Chem.* 49 (2), 81–115. [https://doi.org/10.1016/0304-4203\(95\)00008-F](https://doi.org/10.1016/0304-4203(95)00008-F).
- Herbert, T.D., Dalton, C.A., Liu, Z., Salazar, A., Si, W., Wilson, D.S., 2022. Tectonic degassing drove global temperature trends since 20 Ma. *Science* 377 (6601), 116–119. <https://doi.org/10.1126/science.abl4353>.
- Van Hoang, L., Clift, P.D., Schwab, A.M., Huuse, M., Nguyen, D.A., Zhen, S., 2010. Large-scale erosional response of SE Asia to monsoon evolution reconstructed from sedimentary records of the Song Hong-Yinggehai and Qiongdongnan basins, South China Sea. *Geol. Soc. (Lond.) Spec. Publ.* 342 (1), 219–244. <https://doi.org/10.1144/SP342.13>.
- Hodell, D.A., Woodruff, F., 1994. Variations in the strontium isotopic ratio of seawater during the Miocene: stratigraphic and geochemical implications. *Paleoceanography* 9 (3), 405–426. <https://doi.org/10.1029/94PA00292>.
- Holbourn, A., Kuhnt, W., Lyle, M., Schneider, L., Romero, O., Andersen, N., 2014. Middle Miocene climate cooling linked to intensification of eastern equatorial Pacific upwelling. *Geology* 42 (1), 19–22. <https://doi.org/10.1130/G34890.1>.
- Hornafius, J.S., 1991. Facies analysis of the Monterey Formation in the northern Santa Barbara Channel. *AAPG Bull.* 75 (5), 894–909.
- Hornafius, J.S. (Ed.), 1994. *Field Guide to the Monterey Formation Between Santa Barbara and Gaviota*. AAPG Pacific Section, Bakersfield, CA, California, 123 p.
- Ibach, L.E.J., 1982. Relationship between sedimentation rate and total organic carbon content in ancient marine sediments. *AAPG Bull.* 66 (2), 170–188. <https://doi.org/10.1306/03B59A5D-16D1-11D7-8645000102C1865D>.
- Isaacs, Caroline M., 1981. Porosity reduction during diagenesis of the Monterey Formation, Santa Barbara coastal area, California. In: Garrison, R.E., Douglas, R.G., Piscesotto, K.E., Isaacs, C.M., Ingle, J.C. (Eds.), *The Monterey Formation and Related Siliceous Rocks of California*. Pacific Section, Soc. of Economic Paleontologists and Mineralogists, Los Angeles, CA, pp. 257–271.
- Isaacs, C.M., 1983. Compositional variation and sequence in the Miocene Monterey Formation, Santa Barbara coastal area, California. In: Larue, D.K., Steel, R.J. (Eds.), *Cenozoic Marine Sedimentation, Pacific Margin*. Pacific Section, Soc. Econ. Paleo. Min., Bakersfield, USA, pp. 117–132.
- Isaacs, C.M., 1984. Hemipelagic deposits in a Miocene basin, California: toward a model of lithologic variation and sequence. *Geol. Soc. (Lond.) Spec. Publ.* 15 (1), 481–496. <https://doi.org/10.1144/GSL.SP.1984.015.01.31>.
- Isaacs, C.M., Pollastro, R.M., Barron, J.A., Ingle Jr., J.C., Bukry, D., Dunbar, R.B., Keller, M.A., Tomson, J.H., Lewan, M.D., 2001. Geologic and paleontologic features of rock samples in the cooperative Monterey organic geochemistry study, Naples Beach and Lions Head Sections, California. In: Isaacs, C.M., Rulkötter, J. (Eds.), *The Monterey Formation: From Rocks to Molecules*. Columbia University Press, New York, pp. 373–392.
- Jahnke, R.A., 1990. Early diagenesis and recycling of biogenic debris at the seafloor, Santa Monica Basin, California. *J. Mar. Res.* 48 (2), 413–436. <https://doi.org/10.1357/002224090784988773>.
- John, C.M., Follmi, K.B., De Kaenel, E., Adatte, T., Steinmann, P., Badertscher, C., 2002. Carbonaceous and phosphate-rich sediments of the Miocene Monterey Formation at El Capitan State Beach, California, USA. *J. Sediment. Res.* 72 (2), 252–267. <https://doi.org/10.1306/080701720252>.
- Kasbohm, J., Schoene, B., 2018. Rapid eruption of the Columbia River flood basalt and correlation with the mid-Miocene climate optimum. *Sci. Adv.* 4 (9), 8223. <https://doi.org/10.1126/sciadv.aat8223>.
- Katz, M.E., Wright, J.D., Miller, K.G., Cramer, B.S., Fennel, K., Falkowski, P.G., 2005. Biological overprint of the geological carbon cycle. *Mar. Geol.* 217 (3–4), 323–338. <https://doi.org/10.1016/j.margeo.2004.08.005>.
- Kennedy, M.J., Pevear, D.R., Hill, R.J., 2002. Mineral surface control of organic carbon in black shale. *Science* 295 (5555), 657–660. <https://doi.org/10.1126/science.1066611>.
- Knott, J.R., Sarna-Wojcicki, A.M., Barron, J.A., Wan, E., Heizler, L., Martinez, P., 2022. Tephrochronology of the Miocene Monterey and Modelo Formations, California. In: *Understanding the Monterey Formation and Similar Biosiliceous Units Across Space and Time*, vol. 556, p. 187.
- Kump, L.R., Arthur, M.A., 1999. Interpreting carbon-isotope excursions: carbonates and organic matter. *Chem. Geol.* 161 (1–3), 181–198.
- Kuypers, M.M., Pancost, R.D., Nijenhuis, I.A., Sinnighe Damsté, J.S., 2002. Enhanced productivity led to increased organic carbon burial in the euxinic North Atlantic basin during the late Cenomanian oceanic anoxic event. *Paleoceanography* 17 (4), 3. <https://doi.org/10.1029/2000PA000569>.
- Lallier-Verges, E., Bertrand, P., Desprairies, A., 1993. Organic matter composition and sulfate reduction intensity in Oman margin sediments. *Mar. Geol.* 112 (1–4), 57–69. [https://doi.org/10.1016/0025-3227\(93\)90161-N](https://doi.org/10.1016/0025-3227(93)90161-N).
- Laurent, D., de Kaenel, E., Spangenberg, J.E., Föllmi, K.B., 2015. A sedimentological model of organic-matter preservation and phosphogenesis in the Miocene

- Monterey Formation at Haskells Beach, Goleta (central California). *Sediment. Geol.* 326, 16–32. <https://doi.org/10.1016/j.sedgeo.2015.06.008>.
- Li, Z., Zhang, Y.G., Torres, M., Mills, B.J., 2023. Neogene burial of organic carbon in the global ocean. *Nature* 613 (7942), 90–95. <https://doi.org/10.1038/s41586-022-05413-6>.
- Luyendyk, B.P., Kamerling, M.J., Terres, R., 1980. Geometric model for Neogene crustal rotations in southern California. *Geol. Soc. Am. Bull.* 91 (4), 211–217. [https://doi.org/10.1130/0016-7606\(1980\)91<211:GMFNCR>2.0.CO;2](https://doi.org/10.1130/0016-7606(1980)91<211:GMFNCR>2.0.CO;2).
- Marsaglia, K.M., Davis, A.S., Rinkus, K., Clague, D.A., 2006. Evidence for interaction of a spreading ridge with the outer California borderland. *Mar. Geol.* 229 (3), 259–272. <https://doi.org/10.1016/j.margeo.2006.02.006>.
- Miller, K.G., Browning, J.V., Schmelz, W.J., Kopp, R.E., Mountain, G.S., Wright, J.D., 2020. Cenozoic sea-level and cryospheric evolution from deep-sea geochemical and continental margin records. *Sci. Adv.* 6 (20), eaaz1346. <https://doi.org/10.1126/sciadv.aaz1346>.
- Modestou, S.E., Leutert, T.J., Fernandez, A., Lear, C.H., Meckler, A.N., 2020. Warm middle Miocene Indian Ocean bottom water temperatures: comparison of clumped isotope and Mg/Ca-based estimates. *Paleoceanogr. Paleoclimatol.* 35 (11), e2020PA003927. <https://doi.org/10.1029/2020PA003927>.
- Mollenhauer, G., Schneider, R.R., Müller, P.J., Spieß, V., Wefer, G., 2002. Glacial/interglacial variability in the Benguela upwelling system: spatial distribution and budgets of organic carbon accumulation. *Glob. Biogeochem. Cycles* 16 (4), 81. <https://doi.org/10.1029/2001GB001488>.
- Park, Y., Maffre, P., Goddérus, Y., Macdonald, F.A., Anttila, E.S., Swanson-Hysell, N.L., 2020. Emergence of the southeast Asian islands as a driver for Neogene cooling. *Proc. Natl. Acad. Sci.* 117 (41), 25319–25326. <https://doi.org/10.1073/pnas.2011033117>.
- Pisciotto, K.A., Garrison, R.E., 1981. Lithofacies and depositional environments of the Monterey Formation, California. In: Garrison, R.E., Douglas, R.G., Pisciotto, K.E., Isaacs, C.M., Ingle, J.C. (Eds.), *The Monterey Formation and Related Siliceous Rocks of California. Pacific Section, Soc. of Economic Paleontologists and Mineralogists*, Los Angeles, CA, pp. 97–122.
- Reimers, C.E., Jahnke, R.A., McCorkle, D.C., 1992. Carbon fluxes and burial rates over the continental slope and rise off central California with implications for the global carbon cycle. *Glob. Biogeochem. Cycles* 6 (2), 199–224. <https://doi.org/10.1029/92GB00105>.
- Rothwell, R.G., Croudace, I.W., 2015. Twenty years of XRF core scanning marine sediments: what do geochemical proxies tell us? In: *Micro-XRF Studies of Sediment Cores: Applications of a non-destructive tool for the environmental sciences*. Springer, Dordrecht, pp. 25–102.
- Scheirer, A.H., Magoon, L.B., 2007. Age, distribution, and stratigraphic relationship of rock units in the San Joaquin Basin Province, California. In: *Petroleum Systems and Geologic Assessment of Oil and Gas in the San Joaquin Basin Province. US Geological Survey Professional Paper*, California.
- Schoene, B., Eddy, M.P., Samperton, K.M., Keller, C.B., Keller, G., Adatte, T., Khadri, S.F., 2019. U-Pb constraints on pulsed eruption of the Deccan Traps across the end-Cretaceous mass extinction. *Science* 363 (6429), 862–866. <https://doi.org/10.1126/science.aau2422>.
- Shields, G.A., Mills, B.J., 2017. Tectonic controls on the long-term carbon isotope mass balance. *Proc. Natl. Acad. Sci.* 114 (17), 4318–4323. <https://doi.org/10.1073/pnas.1614506114>.
- Steinhorstottir, M., Coxall, H.K., De Boer, A.M., Huber, M., Barbolini, N., Bradshaw, C.D., Burls, N.J., Feakins, S.J., Gasson, E., Henderiks, J., Holbourn, A.E., 2021. The Miocene: the future of the past. *Paleoceanogr. Paleoclimatol.* 36 (4), e2020PA004037. <https://doi.org/10.1029/2020PA004037>.
- Sosdian, S.M., Babila, T.L., Greenop, R., Foster, G.L., Lear, C.H., 2020. Ocean carbon storage across the middle Miocene: a new interpretation for the Monterey Event. *Nat. Commun.* 11 (1), 134. <https://doi.org/10.1038/s41467-019-13792-0>.
- Vincent, E., Berger, W.H., 1985. *Carbon Dioxide and Polar Cooling in the Miocene: The Monterey Hypothesis. The Carbon Cycle and Atmospheric CO<sub>2</sub>: Natural Variations Archean to Present*, vol. 32, pp. 455–468.
- Westerhold, T., Marwan, N., Drury, A.J., Liebrand, D., Agnini, C., Anagnostou, E., Barret, J.S., Bohaty, S.M., De Vleeschouwer, D., Florindo, F., Frederichs, T., 2020. An astronomically dated record of Earth's climate and its predictability over the last 66 million years. *Science* 369 (6509), 1383–1387. <https://doi.org/10.1126/science.aba6853>.
- Wu, X., Baas, J.H., Parsons, D.R., Eggenhuisen, J., Amoudry, L., Cartigny, M., McLellan, S., Mouazé, D., Ruessink, G., 2018. Wave ripple development on mixed clay-sand substrates: effects of clay winnowing and armoring. *J. Geophys. Res., Earth Surf.* 123 (11), 2784–2801. <https://doi.org/10.1029/2018JF004681>.